RESEARCH Open Access



JNK pathway suppression mediates insensitivity to combination endocrine therapy and CDK4/6 inhibition in ER+ breast cancer

Sarah Alexandrou^{1,2}, Christine S. Lee¹, Kristine J. Fernandez¹, Celine E. Wiharja¹, Leila Eshraghi^{1,2}, John Reeves¹, Daniel A. Reed^{1,2}, Neil Portman^{1,2}, Zoe Phan^{1,2}, Heloisa H. Milioli^{1,2}, Iva Nikolic³, Antonia L. Cadell^{1,2}, David R. Croucher^{1,2}, Kaylene J. Simpson^{3,4}, Elgene Lim^{1,2}, Theresa E. Hickey⁵, Ewan K. A. Millar^{6,7}, Carla L. Alves⁸, Henrik J. Ditzel^{8,9} and C. Elizabeth Caldon^{1,2*}

Abstract

CDK4/6 inhibitors in combination with endocrine therapy are now used as front-line treatment for patients with estrogen-receptor positive (ER+) breast cancer. While this combination improves overall survival, the mechanisms of disease progression remain poorly understood. Here, we performed unbiased genome-wide CRISPR/Cas9 knockout screens using endocrine sensitive ER+ breast cancer cells to identify novel drivers of resistance to combination endocrine therapy (tamoxifen) and CDK4/6 inhibitor (palbociclib) treatment. Our screens identified the inactivation of JNK signalling, including loss of the kinase MAP2K7, as a key driver of drug insensitivity. We developed multiple CRISPR/Cas9 knockout ER+ breast cancer cell lines (MCF-7 and T-47D) to investigate the effects of MAP2K7 and downstream MAPK8 and MAPK9 loss. MAP2K7 knockout increased metastatic burden in vivo and led to impaired JNK-mediated stress responses, as well as promoting cell survival and reducing senescence entry following endocrine therapy and CDK4/6 inhibitor treatment. Mechanistically, this occurred via loss of the AP-1 transcription factor c-JUN, leading to an attenuated response to combination endocrine therapy plus CDK4/6 inhibition. Furthermore, analysis of clinical datasets found that inactivation of the JNK pathway was associated with increased metastatic burden, and low pJNK^{T183/Y185} activity correlated with a poorer response to systemic endocrine and CDK4/6 inhibitor therapies in both early-stage and metastatic ER+ breast cancer cohorts. Overall, we demonstrate that suppression of JNK signalling enables persistent growth during combined endocrine therapy and CDK4/6 inhibition. Our data provides the pre-clinical rationale to stratify patients based on JNK pathway activity prior to receiving combination endocrine therapy and CDK4/6 inhibition.

Statement of translational relevance

Combined use of endocrine therapy and CDK4/6 inhibition is now standard-of-care for patients with ER+ breast cancer, including those with high-risk early-stage and advanced disease. However, insensitivity or resistance to

*Correspondence: C. Elizabeth Caldon I.caldon@garvan.org.au

Full list of author information is available at the end of the article



this therapeutic combination presents a growing clinical challenge as the mechanisms driving drug insensitivity remain poorly understood. Here, we have identified inactivation of JNK signalling, specifically loss of the JNK kinase *MAP2K7*, as a major determinant of insensitivity to combined endocrine therapy and CDK4/6 inhibition in ER+ breast cancer. We uncovered that *MAP2K7* loss augments tumour survival in vitro and in vivo. This occurs via disruption of activator protein-1 (AP-1) transcription factors, and thus prevents the induction of therapy-induced senescence and JNK-activated stress response. These findings reveal a critical tumour suppressor role for the JNK pathway in ER+ breast cancer and suggests that patients with deficient JNK signalling may derive limited benefit from combination endocrine therapy plus CDK4/6 inhibition. This supports the rationale for pre-treatment assessment of JNK pathway activity and cautions against the development of JNK inhibitors for this setting.

Keywords CDK4/6 inhibition, Palbociclib, ER+ breast cancer, JNK signalling, Endocrine therapy

Introduction

The addition of cyclin-dependent kinase 4/6 (CDK4/6) inhibitors (e.g. palbociclib, ribociclib, abemaciclib) to endocrine therapy (e.g. tamoxifen, aromatase inhibitors, fulvestrant) has transformed the treatment landscape for patients with advanced/metastatic estrogen receptor positive (ER+) breast cancer [1-3]. Combination therapy, in first-line and second-line settings, has led to a clinical improvement in overall survival of patients with endocrine sensitive and endocrine refractory disease [4-8] and it is expected that all patients with advanced disease will likely receive combination endocrine and CDK4/6 inhibitor therapy during the course of their treatment. The success of CDK4/6 inhibitors in the advanced setting has encouraged their evaluation in early breast cancer. Ribociclib and abemaciclib have improved invasive-disease free survival in combination with endocrine therapy and have been approved for use in early-stage high-risk ER+ disease [9, 10].

While highly effective for several years, combination endocrine therapy and CDK4/6 inhibition is not curative, and disease inevitably progresses [11]. With the increased use of this combination in the early breast cancer setting, a clinical need exists to identify patients at risk of progressing on treatment. Contemporary studies have identified putative "drivers" for CDK4/6 inhibitor resistance such as Rb loss, FAT1 loss, CDK6 gain or cyclin E1 gain [12–14]. However, these mechanisms have been validated in only a small number of patients, possibly due to the predominance of pre-clinical studies using CDK4/6 inhibitors as single agents. Although preclinical studies of endocrine monotherapy resistance and CDK4/6 inhibitor monotherapy resistance are available, pre-clinical studies of combination endocrine therapy and CDK4/6 inhibitor resistance mechanisms are rare. Therefore, there is an urgent need for studies utilising combination therapies that mimic clinical practice to be employed to study resistance mechanisms.

In this study we identified genes whose loss-of-function leads to insensitivity to combination endocrine and CDK4/6 inhibitor therapy in ER+ breast cancer models using human genome-wide CRISPR/Cas9 screens. We

identified the c-Jun N-terminal kinase (JNK) pathway as a major determinant of resistance to endocrine therapy and CDK4/6 inhibition in this context. The lead hit was MAP2K7, a kinase that directly phosphorylates JNK to control JNK pathway activation. Loss of the JNK pathway, particularly MAP2K7, impaired the anti-proliferative and pro-senescent response of cancer cells to endocrine therapy and CDK4/6 inhibition. Moreover, these cells have an impaired JNK-mediated stress response. Finally, we demonstrated that low expression of MAP2K7 and $\mathsf{pINK}^{\mathrm{T183/Y185}}$ was associated with poor outcomes in early and metastatic ER+ breast cancer patients treated with endocrine therapy and CDK4/6 inhibition. Our findings strongly suggest that the JNK pathway acts as a tumour suppressor in ER+ breast cancer, and that JNK pathway status may be a biomarker of response to combination endocrine and CDK4/6 inhibitor therapy.

Materials and methods

Cell lines and drug treatment

MCF-7 and T-47D cells were cultured in phenol-red free RPMI 1640 (Gibco) supplemented with 5% charcoal-stripped fetal bovine serum (FBS), 1% penicillin/streptomycin (Invitrogen) and 10 pM 17 β -estradiol (E2758; Sigma-Aldrich; resuspended in absolute ethanol (EtOH)). HEK293T cells were cultured in DMEM (Gibco) supplemented with 10% FBS. All cell lines were cultured for less than 6 months after short-tandem repeat profiling (Garvan Molecular Genetics, Garvan Institute of Medical Research (GIMR)), and routinely tested negative for mycoplasma contamination. Cells were cultured under 5% CO₂ in a humidified incubator at 37°C.

The MCF-7 and T-47D MAP2K7-/-, MCF-7 MAPK8-/- and MCF-7 MAPK9-/- cell lines were generated from MCF-7-Cas9- or T-47D-Cas9-expressing cells, and transduced with guide RNAs (gRNAs) targeting MKK7 (MAP2K7), JNK1 (MAPK8) or JNK2 (MAPK9). MAP2K7, MAPK8 and MAPK9 gRNAs in pLentiGuide-Puro were purchased from GenScript. The gRNA sequences were: MKK7_1 ACGGGCTACCTGACCATCGG, MKK7_3 C ATTCTGGGCAAGATGACAG, MAPK8 TCGCTACT ACAGAGCACCCG and MAPK9 AATGGATGCTAA

CTTATGTC. Sequences for the *MAP2K7* gRNAs were chosen based on high enrichment in the pooled CRISPR/ Cas9 screens.

Cells were treated with 300 nM anisomycin (A9789; Sigma-Aldrich; resuspended in dimethyl sulfoxide (DMSO)), 10 μ M venetoclax (S8048; Selleckchem; resuspended in DMSO), and various concentrations of 4-hydroxytamoxifen (H7904; Sigma-Aldrich; resuspended in tetrahydrofuran), fulvestrant (I4409; Sigma-Aldrich; resuspended in EtOH) and palbociclib (S1116; Selleckchem; resuspended in water), as indicated in the figure legends.

In vivo analysis of metastatic burden Xenograft model

All animal work was performed in compliance with the Australian Code of Practice for the Care and Use of Animals for Scientific Purposes (National Health and Medical Research Council). The protocol and study end points were approved by the St. Vincent's Health Precinct and GIMR Animal Ethics Committee (ARA 21/09). Immunocompromised NOD-SCID-IL2γ^{-/-} 5–6 week old female mice were housed in ventilated cages and specific pathogen-free conditions in a 12:12 h light:dark cycle with food and water given ad libitum. After an acclimatisation period of a minimum of seven days, 10 mice per arm were injected via the tail vein with 1.5×10^6 MCF-7 pLenti and MAP2K7^{-/-} (MKK7_3) cells. Cell growth was supported by 17β-estradiol (2.5 µg/mL), administered in the drinking water. Mice were monitored for 9 weeks, with twice weekly bladder palpation to monitor for estradiol toxicity, until ethical endpoint for metastatic burden was reached. Mice were euthanised with isoflurane anaesthetisation and cervical dislocation, and the lungs were harvested and fixed for 24 h in 10% neutral buffered formalin before being transferred to 70% ethanol.

Immunohistochemistry (IHC) and quantification (cytokeratin)

Formalin-fixed paraffin-embedded (FFPE) sections from mouse lung tissue were cut with a microtome, mounted on Epredia SuperFrost slides and dried at 60 °C. Sections were deparaffinised and stained using the Bond RX Automated Stainer (Leica Biosystems). For cytokeratin staining, heat-induced antigen retrieval was performed at pH9 (Bond Epitope Retrieval Solution 2, Leica Biosystems), 100 °C for 30 min, before antibody incubation (1:500; MA1-12594; Thermo Fisher Scientific) for 30 min. Detection was performed with diaminobenzidine (DAB, EnVision Detection Systems, Agilent Dako) and slides were counterstained with haematoxylin. Slides were imaged using a slide scanner (AperioCS2, Leica Biosystems), and images were analysed using QuPath software (version 0.4.4) by manually selecting positively stained regions [15].

Lentiviral production and generation of stable MAP2K7^{-/-}, MAPK8^{-/-} and MAPK9^{-/-} cell lines

HEK293T cells were used to package virus. Plasmids were extracted using the PureLink HiPure Plasmid Filter Maxiprep Kit (Invitrogen) as per the manufacturer's instructions. 4×10^6 HEK293T cells were seeded into 10 cm² plates and transfected with either MAP2K7, MAPK8, or MAPK9 gRNA plasmids, along with packaging plasmids pMDLg/pRRE, pRSV-REV, and pMD2.G. Lentiviral-containing medium was collected 48 h after transfection and filtered using a 0.45 µm filter. MCF-7-Cas9 or T-47D-Cas9 cells were then immediately infected with lentivirus at a 1:2 dilution with 8 μg/mL polybrene (Sigma-Aldrich). Selection with 2 µg/mL puromycin (P8833; Sigma-Aldrich; resuspended in water), occurred 48 h after transduction to generate stably expressing MCF-7-Cas9 and T47-D-Cas9 cell lines including pLenti (empty vector), MKK7_1 and MKK7_3, and MCF-7-Cas9 MAPK8^{-/-} and MAPK9^{-/-} cell lines. Cells were then cultured with a maintenance dose of 1 µg/mL puromycin.

Cell proliferation, clonogenic assays and synchronisation treatments

Metabolic assays were performed in 96-well plates with cells seeded at 1×10^3 cells per well. Cells were treated with drug or vehicle for up to 5 days at the concentrations indicated in the figures, and metabolic rate was assessed using AlamarBlue (Thermo Fisher Scientific). Half-maximal inhibitory concentration (IC₅₀) values were determined using GraphPad Prism software (version 10). Live-cell imaging of cell number was performed using the Incucyte S3 (Live-Cell imaging and Analysis System; Sartorius). 2×10^3 cells per well were seeded in 96-well plates and imaged over 7 days, with 2 fields of view per well. Images were analysed using IncuCyte ZOOM Software (version 2020 C).

For 90-day population size assays, MCF-7 cells were seeded at 4.8×10^6 cells in T150 flasks. Following a 24 h incubation to allow cells to attach, cells were continuously treated with 500 nM palbociclib or 500 nM tamoxifen plus 250 nM palbociclib. Media and drugs were changed every 3–4 days and cells were passaged at 80% confluency. Live cell counts using trypan blue staining (Gibco) were used to calculate cell number to determine population size.

Clonogenic assays were performed in 12-well plates with cells seeded at 3×10^3 cells per well. Drugs were replenished every 3–4 days, for up to 3 weeks. Colonies were fixed with trichloroacetic acid (16%) and stained with 0.1–0.5% crystal violet (Sigma-Aldrich). Plates were scanned using Epson Perfection V800 photo scanner at 1200 dots per inch. Colony area was quantitated using ImageJ software (version 2.1.0/1.53c).

MCF-7 and T-47D pLenti and $MAP2K7^{-/-}$ cells synchronized at G_1/S phase with 48 h 10 nM fulvestrant were released into medium supplemented with 100 nM 17β-estradiol for 12 and 24 h.

Immunoblotting

Cells were lysed in ice-cold Normal Lysis Buffer (10% (v/v) glycerol, 1.2% (w/v) HEPES, 1% (w/v) sodium acid pyrophosphatase, 1% (v/v) Triton X-100, 0.8% (w/v) sodium chloride, 0.4% (w/v) sodium fluoride, 0.04% EGTA, 0.03% (w/v) magnesium chloride) supplemented with 200 μM sodium orthovanadate, 1 mM dithiothreitol, 50 $\mu L/mL$ protease inhibitor cocktail (Sigma-Aldrich) and 10 $\mu g/mL$ MG132. Cell lysates were separated on 4–12% Bis-Tris gels (Invitrogen) as previously described [16].

Primary antibodies used at a 1:1000 dilution were MKK7 (SDC20-87; Invitrogen), MKK4 (PA5-96776; Invitrogen), phospho-JNK^{T183/Y185} (9251; Cell Signalling Technology), JNK (9252; Cell Signalling Technology, detecting JNK2 protein), JNK1 (3708; Cell Signalling Technology), ERα (8644; Cell Signalling Technology), phospho-cJUN^{Ser63} (sc-822; Santa Cruz Biotechnology), cJUN (9165; Cell Signalling Technology) and JUND (5000; Cell Signalling Technology). GAPDH was used at 1:15000 dilution (6C5; Santa Cruz Biotechnology). Secondary antibodies, chemiluminescence and densitometry were performed as previously described [16].

Quantitative real-time polymerase chain reaction (PCR) analysis

Total RNA was extracted from MCF-7 and T-47D pLenti and $MAP2K7^{-/-}$ cell pellets using RNeasy Plus Mini Kit (Qiagen). Reverse transcription was performed using the High-Capacity cDNA Reverse Transcription Kit (Applied Biosystems) to detect mRNA. MAP2K7 (hs00178198_m1), JUN (hs01103582_s1), JUND (hs04187679_s1), ATF3 (hs00231069_m1) and RPLP0 (hs_00420895_gh) Taqman probes (Thermo Fisher Scientific) were used to analyse mRNA expression levels using a QuantStudio7 Flex Real-Time PCR System. Relative gene expression was assessed using the $\Delta\Delta$ Cycle threshold method [17] where expression was normalised to RPLP0.

Senescence associated β-galactosidase assay

Senescence was assessed by visualising β -galactosidase activity using the Senescence β -Galactosidase Staining Kit as per the manufacturer's instructions (Cell Signalling Technology). β -galactosidase activity was imaged using the Leica DFC295 microscope, and the proportion of positive and negative β -galactosidase-stained cells across 3–8 fields of view was quantified using ImageJ Cell Counter.

Flow cytometry

Ethanol-fixed cells were stained with 1 μ g/mL propidium iodide (PI; Sigma-Aldrich) overnight, and incubated with 0.5 mg/mL RNaseA (Sigma-Aldrich) for 2–5 h. Cells were then analysed on a BD FACSCanto II (BD Biosciences). DNA histograms contained ~ 30,000 events, and cell cycle distribution was analysed using FlowJo (version 10.6.1) and ModFit (Verity Software House, version 6.0).

Apoptosis was assessed using the Annexin V-FITC Apoptosis Kit (#K101; BioVision) on the BD FACSCanto II. Cell death by apoptosis was measured by quantifying the proportion of FITC positive/PI negative (early apoptosis) and FITC positive/PI positive (late apoptosis) cells on >30,000 events using FlowJo. Compensation for spectral overlap was performed using an unstained control, a FITC-only control, and a PI-only control (Supplementary Fig. 4G).

Genome-wide pooled CRISPR/Cas9 screens Cas9 cell line generation

MCF-7 and T-47D cells stably expressing Cas9 were generated by transducing cells with Cas9-mCherry lentivirus (Addgene #70182; obtained from the Victorian Centre for Functional Genomics - VCFG) at a multiplicity of infection (MOI) of 0.3. Cas9-mCherry cells were FACS sorted on a BD FACSAria III (BD Biosciences) for the population with the top 10% highest mCherry expression.

Positive selection pooled knockout screens

The human genome-wide pooled Brunello library (containing 77,441 single guide RNAs (sgRNAs)) was provided by the VCFG (Addgene #73178). MCF-7-Cas9 cells were infected with the Brunello library at an MOI of 0.3 using 8 µg/mL polybrene. In parallel, MCF-7-Cas9 cells were used as mock controls and treated only with 8 µg/mL polybrene. 2×10^8 cells were plated at 1×10^6 cells/well in 12-well plates and spin-infected (30 min, 30 °C, 1,200 \times g) to increase lentiviral transduction efficiency. 72 h after infection, Brunello library-transduced and mock-transduced cells were selected with 2 µg/mL puromycin. Functional titre was optimised for the Brunello library to achieve a 22% transduction efficiency.

Following selection, the T_0 baseline timepoint was collected at 1,000-fold representation $(7.6\times10^7~{\rm cells}).$ To ensure the complexity of the Brunello library was maintained at 500-fold representation during treatment (aiming for 500 copies per sgRNA), 3.8×10^7 transduced cells per treatment group was needed at the start of the experiment. Following a 48 h incubation to allow cells to attach, cells were continuously treated with 500 nM tamoxifen plus 250 nM palbociclib (early: 6 week and late: 10 week timepoint) or 500 nM palbociclib alone (early: 2 week and late: 4 week timepoint), supplemented with 1 $\mu \rm g/mL$ puromycin. Media and drugs were changed

every 3–4 days, and cells were expanded at 80% confluency. Importantly, the entire cell population was maintained – no cells were discarded. Pellets of cells were collected for genomic DNA (gDNA) isolation and library preparation at early and late timepoints for each treatment arm across 2 biological replicates.

CRISPR screen sample preparation and sgRNA library sequencing

gDNA was extracted from cell pellets at the early and late timepoints using Midi and Maxi Qiagen Blood and Cell Culture Kits (Qiagen) as per the manufacturer's instructions. PCR amplification and purification of DNA using AMPure beads [18] were then performed as per instructions from VCFG. Before sequencing, Qubit DNA assay was performed for quantification, and a small amount of each sample was run on a 2% agarose gel to confirm the 345 kb PCR product.

Samples were sequenced using 75 bp single-end sequencing at the Molecular Genomics Core facility (Peter MacCallum Cancer Centre) using the Illumina NextSeq 500 platform. Raw FASTQ files were analysed using MAGeCK-VISPR [19] and mapped to the human genome-wide pooled Brunello library (available from h ttps://sourceforge.net/p/mageck/wiki/libraries/). number of mapped reads per sample ranged from 13 million to 19 million, with an average map-ability of 66% (Supplementary Fig. 1A). Sequencing revealed clear differences in the representation of sgRNAs as measured by the Gini index, which is a determinant of inequality among samples (Supplementary Fig. 1B). MAGeCK-MLE (version 0.5.9.3) was used to rank and sort sgRNAs by false discovery rate (FDR) < 0.5 and the results were visualised in VISPR (version 0.4.15) (Supplementary Table 1). Gene set enrichment analysis (GSEA) was performed with MSigDB using Canonical Pathways.

RNAseq data analysis, normalisation and differentially expressed gene (DEG) identification

MCF-7 and T-47D pLenti and *MAP2K7*^{-/-} (MKK7_3) cell lines were treated with either tamoxifen or fulvestrant plus palbociclib for 48 h. Total RNA was extracted from cell pellets as described above. 1 μg RNA was used to prepare libraries using the KAPA mRNA HyperPrep Kit (Roche). Reads were sequenced on a NovaSeq 6000 instrument (Illumina), using 150 bp paired-end sequencing chemistry, by the Sequencing Platform (GIMR).

FASTQ files were quality checked by 'FastQC' (version 0.11.9) [20]. Sequence adaptors and quality filtering was performed using 'AdapterRemoval' (version 2.3.1) and processed paired-end FASTQ reads were aligned to the reference genome assembly 'GRCh38_2020-A_build' [21] using STAR (version 2.7.8) [22] with default parameters. Gene expression was quantified by counting the number

of reads aligned to each Ensembl gene model using 'featureCounts' (version 2.0.1) [23] available through the package *RSubread*.

DEGs between the different treatment groups were identified using the limma-voom method (version 3.46.0) [24, 25]. To normalise read counts according to library size differences between the samples, we used the Trimmed Mean of M-values normalisation method from edgeR (version 3.32.1) [26]. To identify whether the RNAseq library preparation date contributed to variation in gene expression patterns, multidimensional scaling (MDS) was performed on gene expression for all libraries. Genes with low expression were filtered out prior to DEG analysis and only genes with at least 1 count per million reads in the three replicate samples were kept. Genes with FDR adjusted p-value < 0.05 were considered differentially expressed (Supplementary Table 3). Genes that were upregulated or downregulated more than 1-fold with either drug combination (tamoxifen or fulvestrant plus palbociclib) in pLenti cells were identified. These lists were then screened for those genes which showed > 0.25-fold less regulation in MAP2K7^{-/-} cells than in pLenti cells. Genes that showed reduced upregulation or downregulation in MAP2K7^{-/-} cells were analysed by GSEA against the Hallmark datasets using ShinyGo [27].

Transcription factors [28] that had altered expression in $MAP2K7^{-/-}$ cells were identified using a combined cut-off of log fold change > 0.5 between pLenti and $MAP2K7^{-/-}$ cells (Supplementary Table 4). Venn network plots were prepared with EVenn [29].

Clinical samples

Patient demographics and tumour samples

A cohort of 101 metastatic ER+ breast cancer patients treated with combined endocrine therapy and CDK4/6 inhibition with clinical follow-up data were selected as previously described [30]. Of these, 81 had available FFPE material from metastatic lesions for IHC analysis, following which 3 were excluded for lack of identifiable tumour tissue in the sample (Supplementary Fig. 6A).

$Phospho-JNK^{T183/Y185}$ IHC and quantification

FFPE sections from metastatic biopsies were cut with a microtome, mounted on ChemMateTM Capillary Gap Slides (Dako), dried at 60 °C, deparaffinised, and hydrated. Sections were stained using the Bond RX Automated Stainer (Leica Biosystems). For pJNK^{T183/Y185} staining, heat-induced antigen retrieval was performed at pH6 (Bond Epitope Retrieval Solution 1, Leica Biosystems), 100 °C for 20 min, before antibody incubation (1:200; AF1205; R&D Systems) for 60 min. Detection was performed with DAB (Bond Polymer Refine Detection, Leica Biosystems) and slides were counterstained

with haematoxylin. Slides were imaged using the AperioCS2 slide scanner, and images were analysed using QuPath [15]. A semi-quantitative H-score was obtained by the sum of the percentage of tumour cells (0-100%) for each staining intensity (0–3), giving a range of 0 to 300 [31]. H-scores were binned to identify the distribution of expression. Based on the overall distribution of pJNK^{T183/Y185} activity in the cohort (n = 78), thresholds were selected to approximate an even distribution across the three groups: low expression (H-score < 195, n = 25), medium expression (H-score > 195 and < 246, n = 26), and high expression (H-score > 246, n = 27) (Supplementary Fig. 6B).

In silico datasets

Primary and metastatic ER+ breast cancer datasets

Gene expression data was downloaded from The Cancer Genome Atlas (TCGA) [32, 33] through cBioPortal [34, 35] in January and December 2024. The following breast cancer patient cohorts were analysed: Molecular Taxonomy of Breast Cancer International Consortium (METABRIC) [36], TCGA Firehose Legacy [37] and Metastatic Breast Cancer Project (MBCP; provisional dataset) [38]. Each dataset was analysed independently, and ER status was defined as positive by IHC (TCGA and METABRIC) and 'pathology reports' (MBCP). JNK1, JNK2, and pJNK protein expression data from Reverse-Phase Protein Arrays and Clinical Proteomic Tumour Analysis Consortium [39] was obtained from TCGA and UALCAN [40].

Tamoxifen-treated ER+ breast cancers

Array-based gene expression and clinical data from the GSE9893 [41] cohort of tamoxifen-treated ER+ breast cancer patients was downloaded from the Gene Expression Omnibus, NCI database. mRNA expression of Jetset probes [42] was stratified based on metastatic burden. Comparisons were performed using Mann-Whitney unpaired t-test.

Neoadjuvant palbociclib treatment

Gene expression arrays and clinical data from a cohort of early-stage ER+ breast cancer patients treated with preoperative palbociclib for 2 weeks (n=72 samples) was accessed from http://microarrays.curie.fr/publications/U981-GustaveRoussy/pop/ [43]. mRNA expression was stratified into responders and non-responders based on anti-proliferative effect, with responders defined as those showing a significant reduction in proliferation marker TYMS [44].

Statistical analysis

Statistical analysis was performed using GraphPad Prism (version 10). Pairs of datasets were compared using unpaired two-tailed t-tests. Groups of data were

compared using one-way ANOVA followed by multiple comparisons with Tukey's test, two-way ANOVA followed by multiple comparisons with Tukey's test or mixed effects analysis followed by multiple comparisons with Tukey's test. Pearson's analysis was performed to examine correlation between datasets. Kaplan-Meier survival analysis was performed with the Log-rank (Mantel-Cox) test, and hazard ratios were calculated. Violin plots are presented from minimum to maximum, with the range extending from 1st to 3rd quartile, and the line in the middle indicating the median. All experiments were performed in biological triplicate unless otherwise specified. Data are presented as mean ± standard error of the mean (SEM).

Results

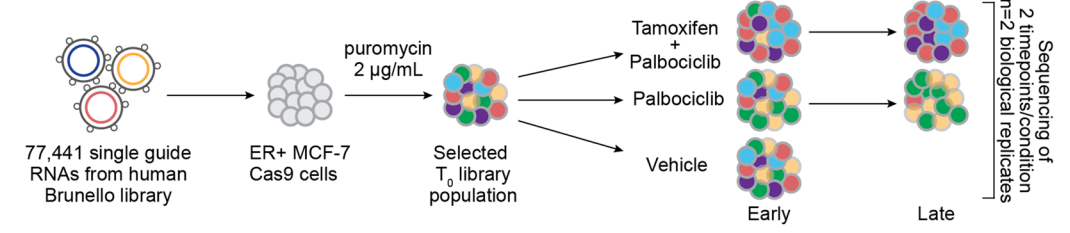
Genome-wide CRISPR/Cas9 screens identify JNK pathway suppression as a driver of endocrine therapy and CDK4/6 inhibitor insensitivity

To identify novel genes conferring insensitivity to combination endocrine therapy and CDK4/6 inhibition in ER+ breast cancer, we performed positive selection (enrichment) genome-wide knockout CRISPR/Cas9 screens in ER+MCF-7 breast cancer cells (Fig. 1A). MCF-7 cells engineered to stably express Cas9 were transduced with the Brunello lentiviral pooled library, which targets 19,114 genes [18]. Following puromycin selection, transduced cells were treated with the combination of 500 nM tamoxifen and 250 nM palbociclib, or 500 nM palbociclib monotherapy (approximate IC₅₀ doses; Supplementary Fig. 1C, D). The combination of tamoxifen and palbociclib was chosen as this clinical strategy provides survival benefit in patients compared to endocrine therapy alone [45]. Moreover, treatment refractory cells emerge within 12 weeks on this treatment combination (Supplementary Fig. 1E), yielding sufficient material for downstream analysis.

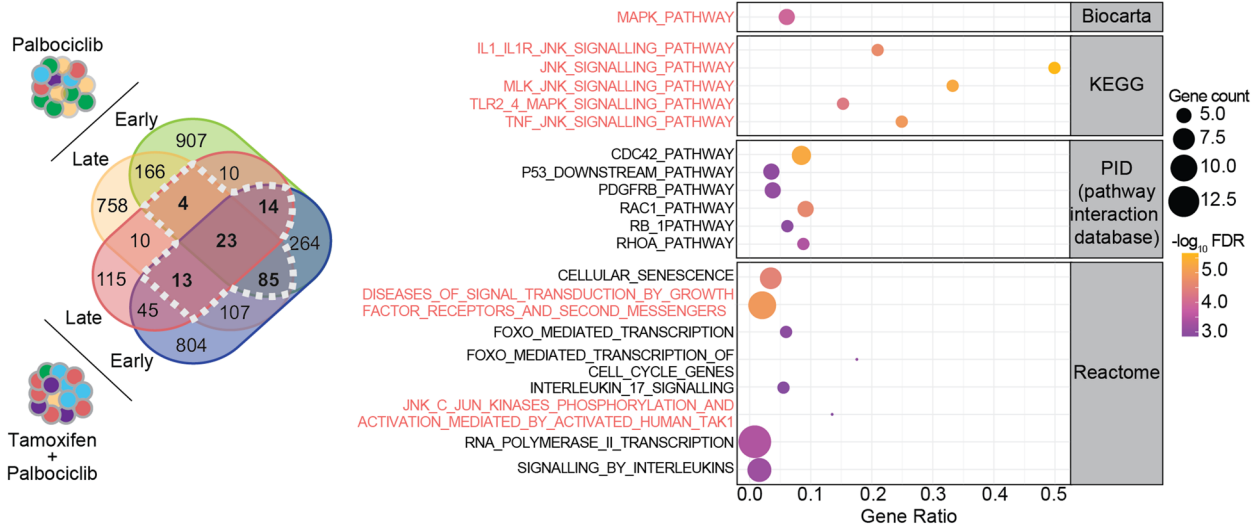
Genomic DNA from each treatment condition was collected after 2/4 weeks (palbociclib arm) and 6/12 weeks (tamoxifen plus palbociclib arm), and sequenced to determine the sgRNA representation compared to the T_0 sgRNA counts using MAGeCK-VISPR [19] (Supplementary Table 1). More than 1.2×10^7 reads were detected per sample, with at least 60% mapped, and Gini analysis showed sgRNA enrichment with selective conditions (Supplementary Fig. 1A, B). Candidate sgRNAs associated with insensitivity to tamoxifen and palbociclib were identified using the inclusion criteria of an FDR < 0.5 and occurrence in at least three screens, including one with the combination therapy (Fig. 1B).

We interrogated a list of 139 genes for known and/ or novel drivers of CDK4/6 inhibitor insensitivity. *RB1*, *CDKN1A* and *PTEN* were significantly enriched and have previously been described to confer resistance to CDK4/6

A CRISPR/Cas9 screen workflow



B Intersecting sgRNA hits C Gene set enrichment

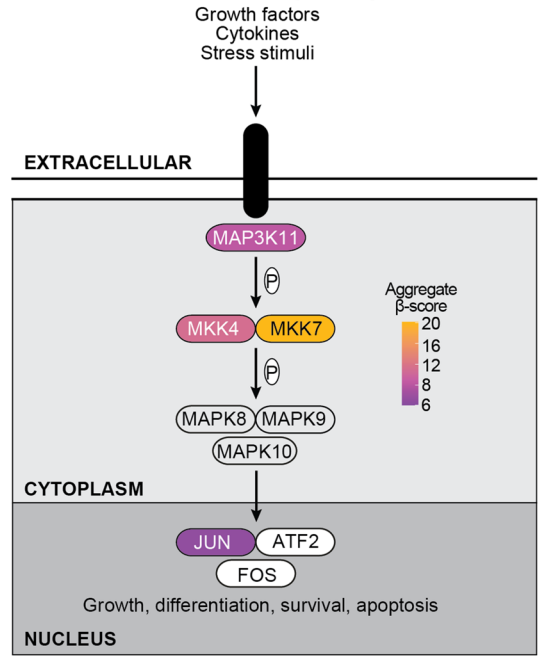


D Top CRISPR/Cas9 hits

		Palbociclib		Tamoxifen + Palbociclib		
	sgRNA	Early	Late	Early	Late	Sum
*	RB1	2.1	8.1	2.6	9.4	22.2
*	MAP2K7	0.91	5.2	5.2	8.8	20.11
*	MAP2K4	0.63	2.8	1.9	5.6	10.93
	FBXO28	1.1	2	3	4.8	10.9
*	PTEN	0.94	1.5	2.2	4.1	8.74
*	MAP3K11	0.4	1.8	1.6	4.5	8.3
	PTPN12	0.54	1.1	0.72	5.8	8.16
	ATXN7L3	0	2.9	1.3	3.3	7.5
	FZR1	0.38	2.3	1.7	2.9	7.28
	NFIB	0.43	1.5	2.2	3.1	7.23
	KEAP1	0.48	0.98	1.6	4.1	7.16
	TIAL1	0.74	2.1	1.5	2.1	6.44
	LZTR1	0.46	1.5	1.5	2.8	6.26
	STK11	0.51	0.92	1.6	3.2	6.23
	CFAP20	0.42	1.5	1.4	2.8	6.12
*	CDKN1A	0.39	2.4	1.3	2	6.09
	NFIC	0.31	0.83	1.7	3.2	6.04
	BCOR	0.55	0	2.2	3.2	5.95
	MEX3D	0.54	0	1.2	4.2	5.94
	RNF41	0.66	1.1	1.3	2.2	5.26
	LCMT1	0	2.1	1	2.1	5.2
	LOC1001321	0	0.84	0.64	3.7	5.18
	ZFR	0.43	0.94	1.2	2.6	5.17
*	JUN	0	1	0.66	3.4	5.06

★ = JNK pathway ★ = known resistance hits

E CRISPR/Cas9 hits in JNK pathway



P = phosphorylation

Fig. 1 (See legend on next page.)

Fig. 1 CRISPR/Cas9 screens identify JNK pathway deficiency in endocrine therapy + CDK4/6 inhibitor insensitive ER+ breast cancer cells. **(A)** CRISPR/Cas9 screens were conducted in ER+ MCF-7-Cas9-expressing cells using the human Brunello library. Cells were treated with the combination of 500 nM tamoxifen and 250 nM palbociclib (early: 6 week and late: 10 week timepoint), or 500 nM palbociclib (early: 2 week and late: 4 week timepoint) or vehicle (tetrahydrofuran) before genomic DNA was collected and sequenced (n = 2 biological replicates). **(B)** Venn diagram showing single guide RNAs (sgRNAs) that increased following treatment with palbociclib and tamoxifen + palbociclib. sgRNAs were selected with a false discovery rate <0.5, and occurrence in ≥3 screens, where at least one screen was with combination therapy. Selected sgRNAs indicated with dashed white line. **(C)** Gene set enrichment analysis of top sgRNAs with ≥2.5 aggregate β-score. **(D)** Top sgRNAs enriched following treatment with palbociclib and tamoxifen + palbociclib, and corresponding β-scores (sgRNAs with aggregate β-score ≥5 are shown). Orange * indicates sgRNAs in the JNK pathway. Black * indicates sgRNAs described in the literature to drive CDK4/6 inhibitor resistance. **(E)** Schematic of the JNK signalling pathway and enriched sgRNAs, as well as aggregate β-score scale. P indicates phosphorylation events

inhibitors [46–50] (Supplementary Table 2). GSEA was performed on the top genes (composite enrichment score \geq 2.5), revealing the involvement of MAPK and JNK signalling pathways (Fig. 1C).

JNK signalling involves a phosphorylation cascade that activates JNK, leading to activation of downstream pathways that modulate proliferation and cell survival. We observed significant depletion across the JNK cascade, including the upstream mediators MAP2K7 (MKK7), MAP2K4 (MKK4), and MAP3K11, the gene that encodes the JNK2 protein (MAPK9), and the downstream transcriptional mediator JUN (Fig. 1D, E; Supplementary Table 2). In our CRISPR/Cas9 screens RB1 was the most enriched gene, however the β-scores were very similar across the two treatment arms (palbociclib composite score: 10.2; tamoxifen plus palbociclib composite score: 12), indicating that insensitivity to CDK4/6 inhibition was primarily driven by RB1 loss (Fig. 1D). MAP2K7 was identified as a top depleted target gene with an aggregate β -score of 20.11 (palbociclib composite score: 6.11; tamoxifen plus palbociclib composite score: 14) (Fig. 1D, E). Interestingly, this result indicates that insensitivity to palbociclib alone or in combination with tamoxifen, is potentially due to MAP2K7 loss and the disruption of JNK signalling. This was surprising as the role of the JNK pathway in cancer is frequently described as oncogenic, although it is reported to act as a tumour suppressor in certain cancer contexts [51].

MAP2K7 loss reduces pJNK^{T183/Y185} activity in ER+ breast cancer

Of the CRISPR/Cas9 target hits, *MAP2K7* was the most enriched sgRNA in the JNK pathway. *MAP2K4* was also highly enriched in our CRISPR screens however, it is known to activate p38 signalling in addition to JNK signalling [52]. This led us to hypothesise that *MAP2K7* (MKK7) is a novel and specific determinant of JNK signalling dysfunction in ER+ breast cancer.

To validate the effects of MAP2K7 loss in ER+ breast cancer, we engineered multiple MAP2K7 CRISPR/Cas9 knockouts in MCF-7 and T-47D cells (MKK7_1 and MKK7_3; Fig. 2A, C) and empty vector pLenti cells. Knockout of MAP2K7 resulted in >97% protein suppression in all $MAP2K7^{-/-}$ MCF-7 and T-47D cell lines

(Fig. 2B, D), without altering MKK4 protein expression (Fig. 2A, C; Supplementary Fig. 2A-D).

Given that the JNK pathway can act as both a tumour suppressor and as an oncogene [53] we first assessed whether MAP2K7 loss would increase tumour burden in vivo. We injected MCF-7 $MAP2K7^{-/-}$ (MKK7_3) knockout cells into the tail-vein of immunocompromised mice, with MCF-7 pLenti cells as a control. After 9 weeks, the lungs of mice were harvested and examined for micrometastases by IHC for human cytokeratin. Mice xenografted with MCF-7 $MAP2K7^{-/-}$ cells incurred, on average, a 2-fold higher number of metastases than those xenografted with MCF-7 pLenti cells (p = 0.008; Fig. 2E), demonstrating that MAP2K7 loss in these cells increased metastatic burden.

We next examined the impact of MAP2K7 loss on JNK phosphorylation. Loss of MAP2K7 resulted in a 75–97% reduction in endogenous pJNK^{T183/Y185} levels in MCF-7 and T-47D cells, indicating that MKK7 mediates a substantial proportion of JNK phosphorylation in proliferating ER+ breast cancer cells (Fig. 2F-I). Loss of MAP2K7 did not alter total JNK protein expression in either MCF-7 or T-47D cells (Fig. 2F, H; Supplementary Fig. 2E-H). We confirmed the co-occurrence of MAP2K7 deletion and low pJNK^{T183/Y185} activity in the TCGA breast cancer cohort (n=616) [32, 37] where JNK phosphorylation was, on average, 37.5% lower in ER+ breast cancers with a MAP2K7 homozygous or heterozygous loss compared to those cancers with no loss of MAP2K7 (diploid, amplified or gain status) (p=0.0002; Fig. 2J).

Since the JNK cascade is activated in response to a range of stress-inducing stimuli [54] we assessed whether *MAP2K7* mediates stress-induced JNK signalling in ER+ breast cancer cells. Using anisomycin, an agent that inhibits protein translation to produce ribotoxic stress [55] JNK phosphorylation was rapidly induced within 30 min, and sustained for 90 min in MCF-7 pLenti cells (Fig. 2K, L; Supplementary Fig. 2I). In contrast, MCF-7 *MAP2K7*^{-/-} cells displayed markedly attenuated JNK phosphorylation within 30 min of anisomycin exposure and pJNK^{T183/Y185} levels returned to basal level by 60 min (Fig. 2L). Quantification of pJNK^{T183/Y185} relative to total protein levels further highlighted the diminished response in *MAP2K7*^{-/-} compared to pLenti cells

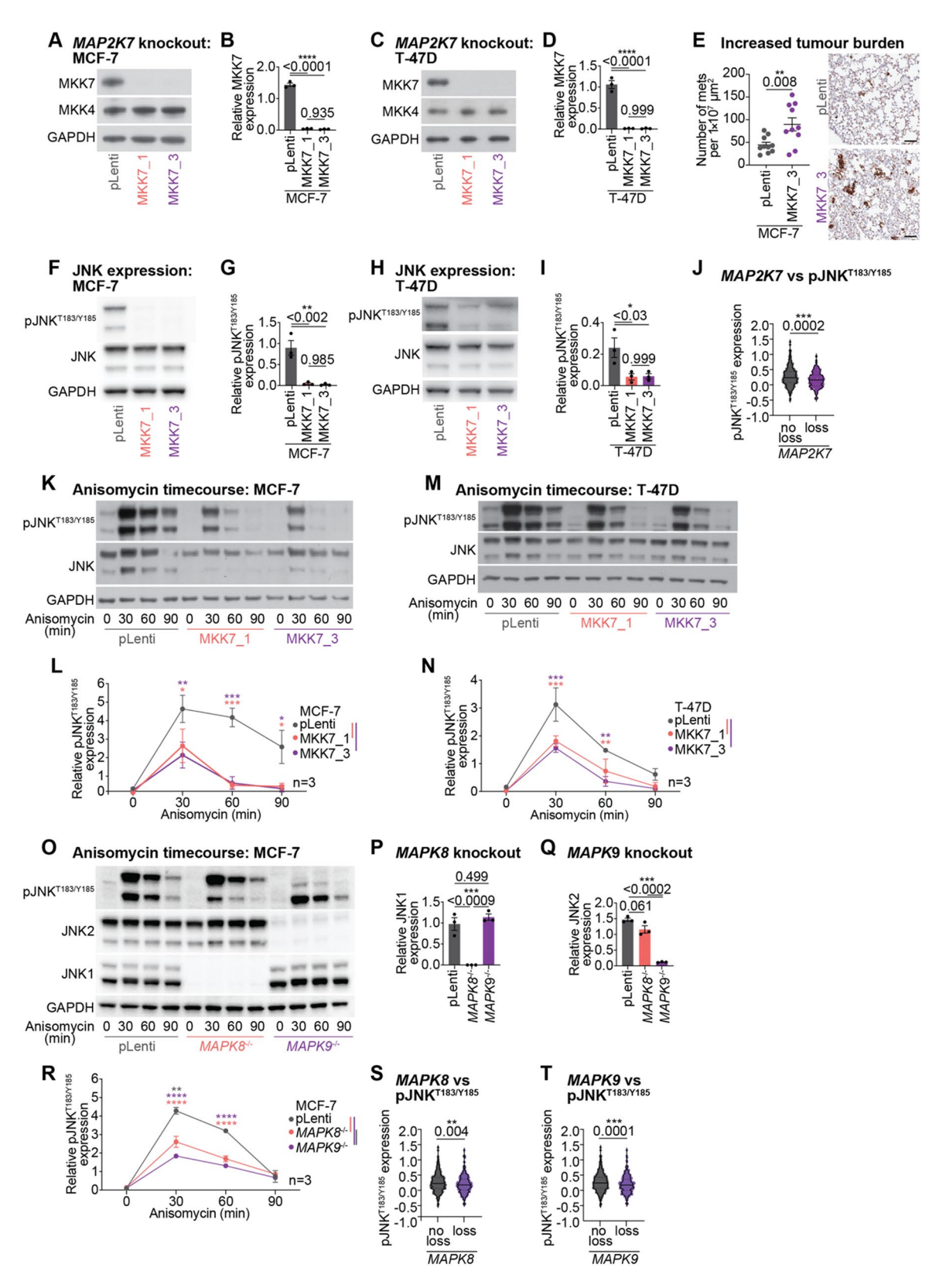


Fig. 2 (See legend on next page.)

Fig. 2 MAP2K7 loss leads to reduced JNK phosphorylation and diminished induction of JNK-induced stress response. (A) Representative Western blot of MKK7, MKK4 and GAPDH in MCF-7 pLenti and MAP2K7^{-/-} (MKK7_1 and MKK7_3) cells (full length blots in Supplementary Fig. 2B). (B) Quantitation of MKK7 expression by densitometry. Band intensity normalised to GAPDH. Data analysed by one-way ANOVA with Tukey's multiple comparisons test. (C) Representative Western blot of MKK7, MKK4 and GAPDH in T-47D pLenti and MAP2K7-/- (MKK7_1 and MKK7_3) cells (full length blots in Supplementary Fig. 2D). (D) Quantitation of MKK7 expression by densitometry. Band intensity normalised to GAPDH. Data analysed by one-way ANOVA with Tukey's multiple comparisons test. (E) Metastases to lung of MCF-7 pLenti and MKK7_3 xenografts (n=10 mice per arm) as measured by cytokeratin immunohistochemistry. Number of metastases (mets) quantitated per 1×10^7 µm² area and analysed by unpaired two-tailed t-test. Representative images shown, scale bar = 200 µm. **(F)** Representative Western blot of pJNK^{T183/Y185}, JNK and GAPDH in MCF-7 pLenti and MAP2K7^{-/-} (MKK7_1 and MKK7_3) cells (full length blots in Supplementary Fig. 2F). (G) Quantitation of pJNK^{T183}/Y¹⁸⁵ activity by densitometry. Band intensity normalised to GAPDH. Data analysed by one-way ANOVA with Tukey's multiple comparisons test. (H) Representative Western blot of pJNK^{T183/Y185}, JNK and GAPDH in T-47D pLenti and MAP2K7^{-/-} (MKK7_1 and MKK7_3) cells (full length blots in Supplementary Fig. 2H). (I) Quantitation of pJNK^{T183/Y185} activity by densitometry. Band intensity normalised to GAPDH. Data analysed by one-way ANOVA with Tukey's multiple comparisons test. (J) Expression of pJNK^{T183/Y185} in primary ER+ breast cancers from the TCGA cohort compared to MAP2K7 copy number status. MAP2K7"no loss" (n = 478) includes cancers with amplified, gain or diploid status for MAP2K7. MAP2K7" (n = 138) includes cancers with heterozygous or homozygous deletion of MAP2K7. Data analysed by unpaired two-tailed t-test. (K) Representative Western blot of pJNK^{T183/Y185}, JNK and GAPDH in MCF-7 pLenti and MAP2K7^{-/-} (MKK7_1 and MKK7_3) cells treated with 300 nM anisomycin for 0, 30, 60, 90 min (full length blots in Supplementary Fig. 2l). (L) Quantitation of pJNK^{T183/Y185} activity by densitometry. Band intensity normalised to GAPDH. Data analysed by two-way ANOVA with Tukey's multiple comparisons test. (M) Representative Western blot of pJNK^{T183}/Y¹⁸⁵, JNK and GAPDH in T-47D pLenti and MAP2K7^{-/-} (MKK7 1 and MKK7 3) cells treated with 300 nM anisomycin for 0, 30, 60, 90 min (full length blots in Supplementary Fig. 2K). (N) Quantitation of pJNK^{T183/Y185} activity by densitometry. Band intensity normalised to GAPDH. Data analysed by two-way ANOVA with mixed effects analysis and Tukey's multiple comparisons test. (O) Representative Western blot of pJNK^{T183/Y185}, JNK2 (detected by JNK antibody), JNK1 and GAPDH in CRISPR/Cas9 MCF-7 cell lines: pLenti, MAPK8^{-/-} and MAPK9^{-/-}. Cells were treated with 300 nM anisomycin for 0, 30, 60, 90 min (full length blots in Supplementary Fig. 2M). (P-Q) JNK1 (P) and JNK2 (Q) expression quantitated at 0 min timepoint. Band intensity normalised to GAPDH. Data analysed by one-way ANOVA with Tukey's multiple comparisons test. (R) Quantitation of pJNK^{T183/Y185} activity by densitometry. Band intensity normalised to GAPDH. Data analysed by two-way ANOVA with Tukey's multiple comparisons test. (S-T) Expression of pJNK^{T183/Y185} in primary ER+ breast cancers from the TCGA cohort compared to MAPK8 (S) or MAPK9 (T) copy number status. MAPK8 (n = 488) or MAPK9 (n = 545) "no loss" includes cancers with amplified, gain or diploid status for MAPK8 or MAPK9. MAPK8 (n = 384) or MAPK9 (n = 379) "loss" includes cancers with heterozygous or homozygous deletion of MAPK8 or MAPK9. Data analysed by unpaired two-tailed t-test

following 60 and 90 min of anisomycin exposure (Supplementary Fig. 2J). Anisomycin exposure in T-47D pLenti cells also led to a profound induction of JNK phosphorylation that was attenuated in T-47D *MAP2K7*^{-/-} cells between 30 and 60 min (Fig. 2M, N; Supplementary Fig. 2K, L). In summary, the loss of *MAP2K7* prevented a sustained stress-mediated induction of JNK phosphorylation in MCF-7 cells, while T-47D cells had a dampened response to persistent stress activation.

MAPK9 (encoding JNK2), another potential gene of interest from the CRISPR screens (Supplementary Tables 1 and 2), has similarities with *MAPK8* (encoding JNK1) that are functionally indistinguishable. To discern the effects of the individual genes, we generated *MAPK8* and *MAPK9* CRISPR/Cas9 knockouts in MCF-7 cells. After establishing that these cell lines exhibited almost complete knockout of their respective JNK protein (Fig. 2O-Q), we examined the effect of *MAPK8* and *MAPK9* loss on JNK phosphorylation. Loss of *MAPK8* and *MAPK9* led to a reduction in peak JNK phosphorylation levels 30 min following anisomycin exposure compared to pLenti cells, with a more profound decrease in *MAPK9*^{-/-} compared to *MAPK8*^{-/-} cell lines (Fig. 2O, R; Supplementary Fig. 2M).

Finally, we examined whether JNK phosphorylation was altered in association with MAPK8 (n=872) or MAPK9 (n=924) copy number loss using data from the TCGA cohort [32, 37]. ER+ breast cancers with MAPK8 deletions had on average 21.6% lower JNK activity (Fig. 2S), whereas cancers with MAPK9 deletion had 26.9% lower

JNK phosphorylation than those without *MAPK9* deletions (Fig. 2T). Overall, *MAPK8* and *MAPK9* deletions were associated with a loss of JNK phosphorylation but did not have as profound an effect as *MAP2K7* loss.

Treatment with combination endocrine therapy and CDK4/6 inhibition alters MKK7 expression and JNK phosphorylation

We next examined the response of MAP2K7^{-/-} cell lines to endocrine therapy and CDK4/6 inhibition. We exposed pLenti and MAP2K7^{-/-} MCF-7 and T-47D cells to endocrine therapy (tamoxifen or fulvestrant) plus palbociclib to determine if MKK7 and pJNKT183/Y185 were regulated by the drug combinations (Fig. 3A-F). Tamoxifen plus palbociclib treatment partially reduced MKK7 expression in MCF-7 pLenti cells (Fig. 3B), while treatment with either tamoxifen or fulvestrant plus palbociclib reduced MKK7 protein expression in T-47D pLenti cells (Fig. 3E). MKK7 expression remained undetectable in MAP2K7-/- cells, and MAP2K7 mRNA expression was unaltered with treatment (Fig. 3B, E; Supplementary Fig. 3A, B). pJNK^{T183/Y185} was significantly upregulated in MCF-7 pLenti cells exposed to either tamoxifen or fulvestrant plus palbociclib (Fig. 3C, F). However, only tamoxifen plus palbociclib, and not fulvestrant plus palbociclib treatment led to an increase in JNK activity in T-47D pLenti cells. As before, the level of pJNK^{T183/Y185} was negligible to low in MAP2K7 knockout MCF-7 and T-47D cell lines, and not altered with drug treatment (Fig. 3C, F). In summary, ER+ breast cancer cells exhibit

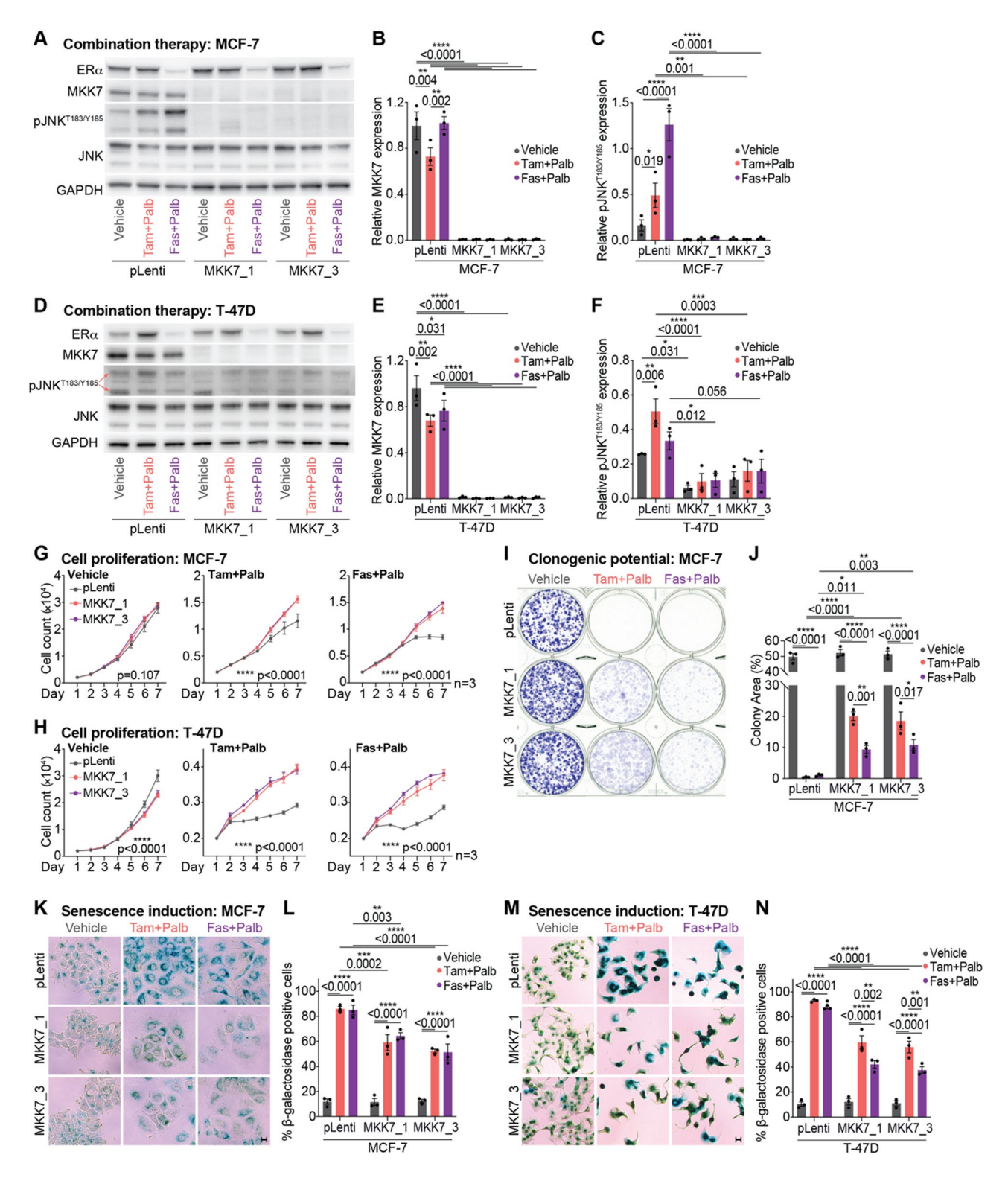


Fig. 3 (See legend on next page.)

Fig. 3 MAP2K7 loss prevents growth arrest and senescence induction following endocrine therapy+CDK4/6 inhibitor treatment (A) Representative Western blot of ERa, MKK7, pJNK^{T183/Y185}, JNK and GAPDH in MCF-7 pLenti and MAP2K7^{-/-} (MKK7_1 and MKK7_3) cells treated with 500 nM tamoxifen + 250 nM palbociclib (tam + palb), 25 nM fulvestrant + 125 nM palbociclib (fas + palb) or vehicle (Absolute ethanol (EtOH) and tetrahydrofuran (THF)) for 48 h (full length blots in Supplementary Fig. 3D). (B) Quantitation of MKK7 expression by densitometry. Band intensity normalised to GAPDH. Data analysed by two-way ANOVA with Tukey's multiple comparisons test. (C) Quantitation of pJNK^{T183/Y185} activity by densitometry. Band intensity normalised to GAPDH. Data analysed by two-way ANOVA with Tukey's multiple comparisons test. (D) Representative Western blot of ERa, MKK7, pJNK^{T183}/Y¹⁸⁵, JNK and GAPDH in T-47D pLenti and MAP2K7^{-/-} (MKK7_1 and MKK7_3) cells treated with 500 nM tamoxifen + 250 nM palbociclib (tam + palb), 25 nM fulvestrant + 125 nM palbociclib (fas + palb) or vehicle (EtOH and THF) for 48 h (full length blots in Supplementary Fig. 3F). (E) Quantitation of MKK7 expression by densitometry. Band intensity normalised to GAPDH. Data analysed by two-way ANOVA with Tukey's multiple comparisons test. (F) Quantitation of pJNK^{T183/Y185} activity by densitometry. Band intensity normalised to GAPDH. Data analysed by two-way ANOVA with Tukey's multiple comparisons test. (G) MCF-7 pLenti and MAP2K7^{-/-} (MKK7_1 and MKK7_3) cells treated with 500 nM tamoxifen + 250 nM palbociclib (tam + palb), 25 nM fulvestrant + 125 nM palbociclib (fas + palb) or vehicle (EtOH and THF) and analysed by time-lapse microscopy using an IncuCyte ZOOM over 7 days. Cell count determined by red fluorescent count, and data analysed by two-way ANOVA with Sidak's multiple comparisons test. Experiment performed in quadruplicate. (H) T-47D pLenti and MAP2K7^{-/-} (MKK7_1 and MKK7_3) cells treated with 500 nM tamoxifen + 250 nM palbociclib (tam + palb), 25 nM fulvestrant + 125 nM palbociclib (fas + palb) or vehicle (EtOH and THF) and analysed by time-lapse microscopy using an IncuCyte ZOOM over 7 days. Cell count determined by red fluorescent count, and data analysed by two-way ANOVA with Sidak's multiple comparisons test. Experiment performed in triplicate. (I) Representative colony formation from MCF-7 pLenti and MAP2K7^{-/-} (MKK7_1 and MKK7_3) cells treated with 500 nM tamoxifen + 250 nM palbociclib (tam + palb), 25 nM fulvestrant + 125 nM palbociclib (fas + palb) or vehicle (EtOH and THF) for 3 weeks, with colony formation detected with 0.1–0.5% crystal violet stain. (J) Colony formation quantitated using ImageJ. Data analysed by two-way ANOVA with Tukey's multiple comparisons test. (K) Representative brightfield images of MCF-7 pLenti and MAP2K7^{-/-} (MKK7_1 and MKK7_3) cells treated with 500 nM tamoxifen + 250 nM palbociclib (tam+palb), 25 nM fulvestrant + 125 nM palbociclib (fas + palb) or vehicle (EtOH and THF) for 72 h and stained with senescence-associated β -galactosidase. (L) Quantification of MCF-7 pLenti and $MAP2K7^{-/-}$ cells staining positive for senescence-associated β -galactosidase from (K). Data analysed by two-way ANOVA with Tukey's multiple comparisons test. Scale bar = 100 µm. (M) Representative brightfield images of T-47D pLenti and MAP2K7^{-/-} (MKK7 1 and MKK7 3) cells treated with 500 nM tamoxifen + 250 nM palbociclib (tam + palb), 25 nM fulvestrant + 125 nM palbociclib (fas + palb) or vehicle (EtOH and THF) for 72 h and stained with senescence-associated β -galactosidase. (N) Quantification of T-47D pLenti and $MAP2K7^{-/-}$ cells staining positive for senescence-associated β -galactosidase from (M). Data analysed by two-way ANOVA with Tukey's multiple comparisons test. Scale bar = 100 μ m

treatment-dependent reductions in MKK7 and $pJNK^{T183/Y185}$ expression.

As we had identified that MAP2K7 sgRNAs were particularly enriched in cells with diminished sensitivity to a therapeutic combination with anti-estrogens, we aimed to assess whether MAP2K7 knockout had an effect on ER α expression and the ability of cells to respond to antiestrogen therapies. MCF-7 and T-47D $MAP2K7^{-/-}$ cells showed similar basal expression of ER α when compared to pLenti cells (Fig. 3A, D; Supplementary Fig. 3C-F). Fulvestrant treatment, as expected, reduced ER α expression > 3-fold compared to vehicle treatment in both cell lines (Supplementary Fig. 3C, E).

MAP2K7 loss promotes proliferation and cell survival following treatment with combination endocrine therapy and CDK4/6 inhibition

Given that *MAP2K7* loss was associated with cell survival in our CRISPR/Cas9 screens, we explored the role of *MAP2K7* in mediating both acute cell cycle regulation, and long-term proliferation and survival in cells treated with endocrine therapy plus palbociclib. We first examined whether *MAP2K7*^{-/-} cells failed to undergo complete cell cycle arrest when treated with endocrine therapy plus palbociclib. All cell lines underwent similar cell cycle arrest, regardless of *MAP2K7* knockout (Supplementary Fig. 3G-I).

Next, we examined whether there were differences in cell number over an extended period using time-lapse microscopy. MCF-7 *MAP2K7*^{-/-} cells showed similar basal rates of cell proliferation as vehicle-treated pLenti

cells (Fig. 3G), while T-47D pLenti cells proliferated slightly faster compared to $MAP2K7^{-/-}$ cells (Fig. 3H). In contrast, $MAP2K7^{-/-}$ cells treated with the combination of endocrine therapy and palbociclib exhibited a significantly higher growth rate compared to pLenti cells (Fig. 3G, H).

We then assessed cell survival of *MAP2K7*^{-/-} cells using colony formation assays. MCF-7 *MAP2K7*^{-/-} cells treated with tamoxifen or fulvestrant plus palbociclib formed significantly more colonies compared to pLentitreated cells (Fig. 3I, J), indicating innate insensitivity to endocrine therapies and CDK4/6 inhibition. T-47D cells treated over the same timeframe did not produce sufficient colonies for analysis.

Given the reduced anisomycin-induced pJNKT183/Y185 activation in MAPK8^{-/-} and MAPK9^{-/-} MCF-7 cells (Fig. 2O, R), we sought to evaluate whether these cells exhibited an altered response to endocrine therapy plus palbociclib treatment. To assess this, we measured changes to cell proliferation over 7 days using an Incu-Cyte assay. pLenti vehicle-treated cells proliferated significantly faster than MAPK8-/- and MAPK9-/- cells (p = 0.0006; Supplementary Fig. 3J). However, knockout of MAPK8 or MAPK9 did not alter growth rates of cells treated with endocrine therapy plus palbociclib compared to pLenti cells (Supplementary Fig. 3J). Overall, MAP2K7, but not MAPK8 or MAPK9 loss was associated with increased growth rates and cell survival following treatment with combination endocrine therapy and palbociclib.

MAP2K7 knockout cells are refractory to senescence when treated with combination endocrine therapy and CDK4/6 inhibition

Since the induction of senescence is a major component of the cytostatic effect of endocrine therapies and CDK4/6 inhibitors [56, 57] we evaluated the impact of MAP2K7 loss on senescence response. We analysed MCF-7 and T-47D $MAP2K7^{-/-}$ cells for senescence by detecting the accumulation of senescence-associated β -galactosidase. Combination therapy led to a 20–50% decrease in the number of $MAP2K7^{-/-}$ knockout cells staining positive for β -galactosidase compared to pLenti cells in both MCF-7 and T-47D cell lines (Fig. 3K-N).

MAP2K7 loss does not alter the induction of apoptosis

Given that activation of the JNK signalling cascade regulates apoptotic signalling [54] we initially hypothesised that the pro-apoptotic function of JNK signalling would be diminished following MAP2K7 knockout in the tumour suppressive ER+ breast cancer context. Characterisation of BCL-2 pro- and anti-apoptotic proteins in pLenti and MAP2K7-/- cells demonstrated no changes to the basal expression of proteins, except for a marginal increase in the expression of the pro-survival protein, BCL-2, in T-47D MAP2K7^{-/-} cells (Supplementary Fig. 4A-D). Next, we used the BCL-2 inhibitor venetoclax, which has been reported to activate JNK expression [58, 59] to evaluate apoptotic induction through annexin V (Supplementary Fig. 4E-G). There were no changes to venetoclax-induced apoptosis in MAP2K7^{-/-} compared to pLenti cells, and inconsistent increases in apoptosis induction between the MCF-7 MAP2K7 sgRNAs (Supplementary Fig. 4E, F).

MAP2K7 loss diminishes the response to endocrine therapy and CDK4/6 inhibition via loss of activator protein-1 (AP-1) transcription factors

We next undertook an unbiased approach, performing RNAseq on MAP2K7 knockout cells to determine how treatment naïve cells responded to acute endocrine therapy plus palbociclib treatment. pLenti and MKK7_3 MCF-7 and T-47D cells were exposed to vehicle, tamoxifen plus palbociclib or fulvestrant plus palbociclib, and analysed by RNAseq (Fig. 4A). MDS was applied to RNAseq data to visualise the relationships between samples based on gene expression profiles. MDS analysis showed that exposure to drug combinations led to significant changes in gene expression in dimension 1 that was dependent on drug treatment in both pLenti and $MAP2K7^{-/-}$ cells, with treatment groups clustering closely together (Fig. 4B, Supplementary Table 3).

We then examined the effect of MAP2K7 loss by mapping the correlation between drug-induced gene regulation in MCF-7 and T-47D pLenti and $MAP2K7^{-/-}$ cells

(Fig. 4C). Gene regulation by tamoxifen or fulvestrant plus palbociclib showed a significant linear correlation between MCF-7 and T-47D pLenti and $MAP2K7^{-/-}$ cells. Remarkably, $MAP2K7^{-/-}$ cells showed an attenuated response in the upregulation and downregulation of the majority of genes affected by combination therapy. This led to a significant shift from perfect correlation (p<0.00001) [60]. Overall, this confirmed that gene expression in response to drug treatment was being attenuated following MAP2K7 knockout, rather than new gene expression programs being induced by MAP2K7 loss.

We examined the attenuated pathways by performing GSEA of genes that were less downregulated or upregulated in MAP2K7^{-/-} cells compared to pLenti cells. We used a cut-off of genes that are more than 1-fold downregulated in pLenti cells, which were then 0.25-fold less downregulated in MAP2K7^{-/-} cells, and examined enrichment of Hallmark gene sets. Using sets of downregulated genes, we identified that the most enriched signatures from each cell line and treatment condition were almost identical, including E2F_TARGETS, G2M_ CHECKPOINT, MITOTIC SPINDLE and ESTRO-GEN_RESPONSE_LATE (Fig. 4D). These are pathways that are regulated downstream of anti-estrogen and CDK4/6 inhibitor treatment [11, 61]. Next, we examined upregulated gene signatures and found that the most consistently attenuated signature with MAP2K7 loss was HALLMARK_TNFA_SIGNALLING_VIA_NFKB, which is a co-regulated pathway in estrogen signalling and in MAPK signalling [62] (Fig. 4D). Overall, MAP2K7 loss attenuated transcriptional pathways controlling cell cycle response during drug treatment.

Surprisingly, we did not see changes to canonical MAPK signalling, which would be detected by signatures involving apoptosis, MAPK and stress response. Consequently, we examined which transcription factors were most differentially regulated by loss of MAP2K7, both before and after drug treatment, to understand how transcriptional regulation is disrupted downstream of endocrine therapy and CDK4/6 inhibitor treatment. Firstly, we examined the difference in expression of transcription factors between vehicle-treated pLenti and MAP2K7-/cells, using a cut-off of log fold change > 0.5. Only two transcription factors, JUN and JUND, were commonly downregulated with MAP2K7 loss in MCF-7 and T-47D cell lines (Fig. 4E). JUN and JUND are both components of AP-1 transcriptional complexes that enable growth factor co-activation of estrogen signalling [63]. Furthermore, JUN was a hit in our CRISPR/Cas9 screens shown in Fig. 1D and E. Following treatment with combination endocrine therapy plus palbociclib, there was a greater number of transcription factors deregulated with MAP2K7 loss in each condition (Fig. 4F). There were 15

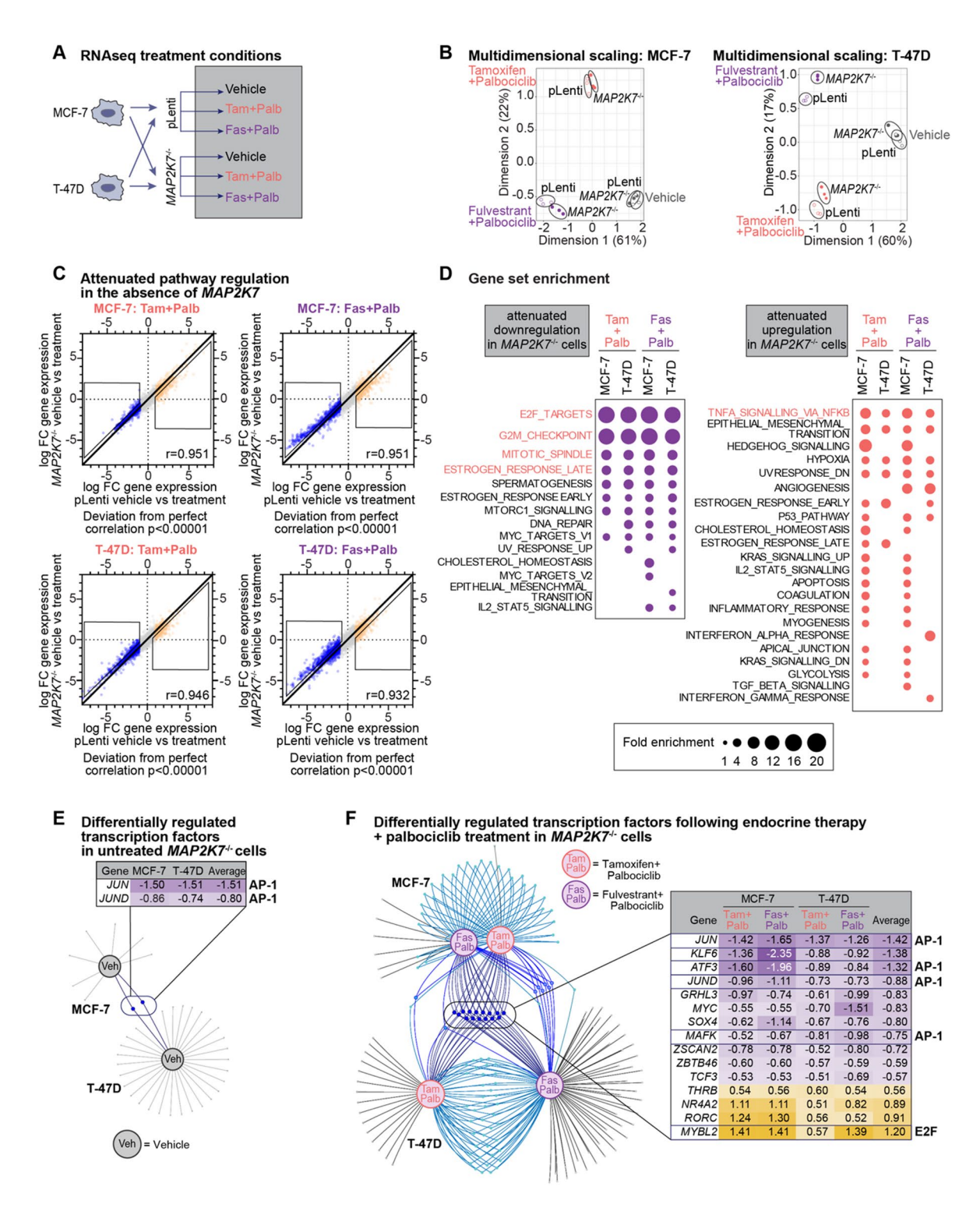


Fig. 4 (See legend on next page.)

Fig. 4 *MAP2K7* loss alters the transcriptional response to endocrine therapy + CDK4/6 inhibitor treatment **(A)** Experimental schematic of pLenti and MKK7_3 cells (MCF-7 or T-47D) treated with 500 nM tamoxifen + 250 nM palbociclib (tam+palb), 25 nM fulvestrant + 125 nM palbociclib (fas + palb) or vehicle (Absolute ethanol (EtOH) and tetrahydrofuran (THF)) for 48 h. RNA collected and analysed by RNAseq. **(B)** Multidimensional scale analysis of RNAseq data of MCF-7 cells +/- treatments, and T-47D cells +/- treatments. **(C)** Relative change in gene expression between vehicle and treatment (tamoxifen + palbociclib or fulvestrant + palbociclib) of $MAP2K7^{-/-}$ vs. pLenti cells. Boxed regions are genes that are less downregulated, or less upregulated, in MKK7_3 cells compared to pLenti cells. Pearson's correlation coefficient shown. **(D)** Analysis of gene set enrichment of hallmark gene sets from genes that show attenuated downregulation (purple dots) or upregulation (orange dots) with treatment in $MAP2K7^{-/-}$ cells, in either MCF-7 or T-47D cell lines. Size of dot is fold enrichment of the signature, with enriched signatures with false discovery rate (FDR) of 0.05. FDR values listed in Supplementary Table 3. **(E)** Venn spider plots of transcription factors (TFs) commonly deregulated in $MAP2K7^{-/-}$ MCF-7 and $MAP2K7^{-/$

common deregulated transcription factors (downregulated transcription factors: *JUN, KLF6, ATF3, JUND, GRHL3, MYC, SOX4, MAFK, ZSCAN2, ZBTB46, TCF3*; upregulated transcription factors: *THRB, NR4A2, RORC, MYBL2*). Of these, four (*JUN, JUND, ATF3* and *MAFK*) were AP-1 component genes.

cJUN transcription factor expression is depleted following MAP2K7 loss

We next validated the relative protein and mRNA expression of AP-1 transcription factor genes in pLenti and MAP2K7-/- MCF-7 and T-47D cells under basal and treatment conditions. Both MCF-7 and T-47D $MAP2K7^{-/-}$ cells showed a marked reduction in p-cJUN-Ser63 and total cJUN protein under basal conditions (Fig. 5A-F). Treatment with tamoxifen or fulvestrant plus palbociclib led to a significant increase in the induction of p-cJUN^{Ser63} activity in both MCF-7 and T-47D cells, but in the absence of MAP2K7, the expression of JUN mRNA and p-cJUN^{Ser63} and cJUN protein remained low or absent (Fig. 5A-F; Supplementary Fig. 5A, B). Quantification of p-cJUN Ser63 relative to cJUN expression supported these findings: p-cJUNSer63 activity was lower in both MCF-7 and T-47D MAP2K7^{-/-} compared to pLenti cells under basal conditions and upon treatment with tamoxifen or fulvestrant plus palbociclib (Supplementary Fig. 5C, E, F, H). However, we did not observe an increase in p-cJUN^{Ser63} activity in pLenti cells treated with endocrine therapy plus palbociclib (Supplementary Fig. 5C, F). JUND mRNA and JUND protein were not altered at basal conditions in MAP2K7^{-/-} compared to pLenti cells, with the exception of a decrease in the expression of JUND in T-47D MKK7_3 cells (Fig. 5A, D; Supplementary Fig. 5A, B; Supplementary Fig. 5D, G). Only treatment with fulvestrant, and not tamoxifen plus palbociclib led to a decrease in JUND protein. However, this was not consistent between MCF-7 and T-47D cell lines and not unique to MAP2K7^{-/-} cells (Supplementary Fig. 5D, G). Surprisingly, the inverse was seen with JUND mRNA expression, where treatment with endocrine therapy plus palbociclib increased expression (Supplementary Fig. 5B).

Two other AP-1 transcription factors were altered in RNAseq analysis: ATF3 and MAFK. ATF3 protein was not detectable by Western blot in MCF-7 and T-47D cells, and mRNA expression was only altered in MCF-7 not T-47D cells (Supplementary Fig. 5A, B). *MAFK* was expressed at very low transcript levels in both MCF-7 and T-47D cells (Supplementary Table 3).

Overall, the loss of *MAP2K7* led to a severe depletion of the AP-1 transcription factor cJUN, which is a fundamental co-factor of the ER. Consequently, we examined whether *MAP2K7* loss altered cell cycle progression in the context of endocrine therapy-induced cell cycle arrest and release (Fig. 5G). All cell lines underwent similar G_1 phase cell cycle arrest with fulvestrant treatment, and estradiol stimulation did not alter cell cycle distribution of *MAP2K7*^{-/-} compared to pLenti cell lines (Supplementary Fig. 5I, J).

Since acute changes in cell cycle response were not observed, we examined whether MAP2K7 loss altered JNK phosphorylation and JUN regulation following ER blockade and stimulation (Fig. 5H, L). In MCF-7 pLenti cells, the addition of fulvestrant led to an increase in pJNKT183/Y185 activity, and this high pJNKT183/Y185 level was maintained in cells stimulated with estradiol (Fig. 5I). Loss of MAP2K7 led to a loss of pJNKT183/Y185 activity with fulvestrant treatment, and estradiol stimulation in MCF-7 cells (Fig. 5I). In T-47D pLenti and MAP2K7^{-/-} cells, the phosphorylation of JNK was maintained in fulvestrant-arrested and estradiol-stimulated cells (Fig. 5M). Fulvestrant-arrested MCF-7 but not T-47D pLenti cells had an increase in p-cJUN^{Ser63} activity and total protein expression compared to asynchronously proliferating cells, which was further enhanced with estradiol stimulation in MCF-7 and T-47D cells (Fig. 5J, K, N, O; Supplementary Fig. 5K, L). MCF-7 MAP2K7^{-/-} cells lacked p-cJUN^{Ser63} activity despite treatment with fulvestrant and estradiol (Fig. 5J; Supplementary Fig. 5K). In contrast, estradiol stimulation but not fulvestrant treatment of T-47D MAP2K7-/- cells led to a decrease in p-cJUN-Ser63 activity compared to treated T-47D pLenti cells (Fig. 5N; Supplementary Fig. 5L). Thus, in this model system JNK and cJUN are phosphorylated by fulvestrant

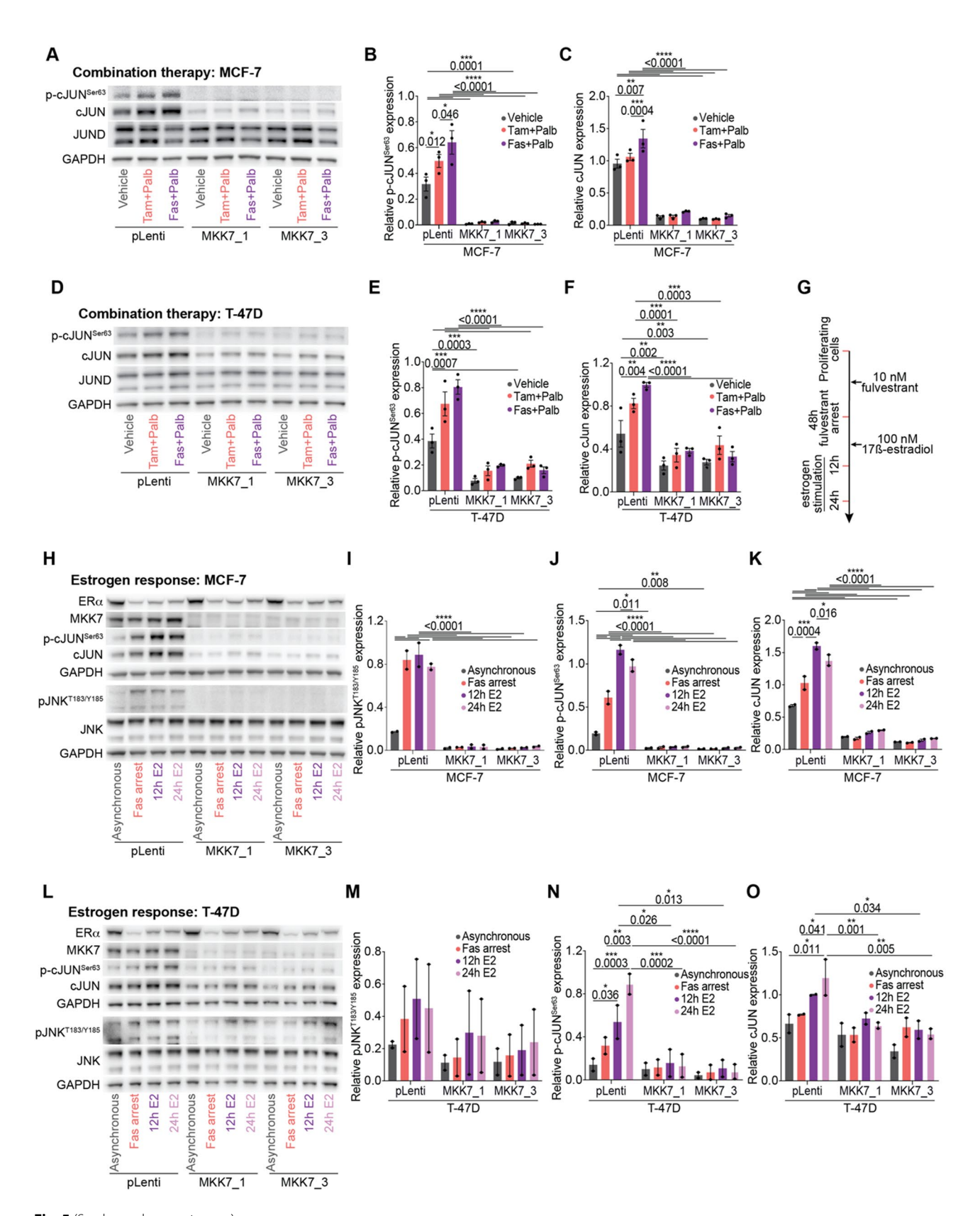


Fig. 5 (See legend on next page.)

Fig. 5 MAP2K7 loss ameliorates AP-1 transcription factor signaling (A) Representative Western blot of p-cJUN^{Ser63}, cJUN, JUND and GAPDH in MCF-7 pLenti and MAP2K7-/- (MKK7_1 and MKK7_3) cells treated with 500 nM tamoxifen + 250 nM palbociclib (tam + palb), 25 nM fulvestrant + 125 nM palbociclib (fas + palb) or vehicle (Absolute ethanol (EtOH) and tetrahydrofuran (THF)) for 48 h (full length blots in Supplementary Fig. 5E). (B) Quantitation of p-cJUN^{Ser63} activity by densitometry. Band intensity normalised to GAPDH. Data analysed by two-way ANOVA with Tukey's multiple comparisons test. (C) Quantitation of cJUN expression by densitometry and normalised to GAPDH. Data analysed by two-way ANOVA with Tukey's multiple comparisons test. (D) Representative Western blot of p-cJUN^{Ser63}, cJUN, JUND and GAPDH in T-47D pLenti and MAP2K7-/- (MKK7_1 and MKK7_3) cells treated with 500 nM tamoxifen + 250 nM palbociclib (tam + palb), 25 nM fulvestrant + 125 nM palbociclib (fas + palb) or vehicle (EtOH and THF) for 48 h (full length blots in Supplementary Fig. 5H). (E) Quantitation of p-cJUN^{Ser63} activity by densitometry. Band intensity normalised to GAPDH. Data analysed by two-way ANOVA with Tukey's multiple comparisons test. (F) Quantitation of cJUN expression by densitometry and normalised to GAPDH. Data analysed by twoway ANOVA with Tukey's multiple comparisons test. (G) Schematic of treatment to examine short-term fulvestrant-mediated arrest and release. MCF-7 and T-47D cells were treated with 10 nM fulvestrant for 48 h to induce a cell cycle arrest. Cells were then stimulated to re-enter the cell cycle with 100 nM 17β-estradiol for 12 h and 24 h. (H) Representative Western blot of ERα, MKK7, p-cJUN^{Ser63}, cJUN, pJNK^{T183/Y185}, JNK and GAPDH in MCF-7 pLenti and MAP2K7^{-/-} (MKK7_1 and MKK7_3) cells treated with 10 nM fulvestrant (fas) and 100 nM 17β-estradiol (E2) (full length blots in Supplementary Fig. 5M). (I) Quantitation of pJNK^{T183/Y185} activity by densitometry. Band intensity normalised to GAPDH. Data analysed by two-way ANOVA with Tukey's multiple comparisons test on duplicate samples. (J) Quantitation of p-cJUN^{Ser63} activity by densitometry. Band intensity normalised to GAPDH. Data analysed by two-way ANOVA with Tukey's multiple comparisons test on duplicate samples. (K) Quantitation of cJUN expression by densitometry. Band intensity normalised to GAPDH. Data analysed by two-way ANOVA with Tukey's multiple comparisons test on duplicate samples. (L) Representative Western blot of ERg, MKK7, p-cJUN^{Ser63}, cJUN, pJNK^{T183/Y185}, JNK and GAPDH in T-47D pLenti and MAP2K7^{-/-} (MKK7 1 and MKK7 3) cells treated with 10 nM fulvestrant (fas) and 100 nM 17β-estradiol (E2) (full length blots in Supplementary Fig. 5N). (M) Quantitation of pJNK^{T183/Y185} activity by densitometry. Band intensity normalised to GAPDH. Data analysed by two-way ANOVA with Tukey's multiple comparisons test on duplicate samples. (N) Quantitation of p-cJUN^{Ser63} activity by densitometry. Band intensity normalised to GAPDH. Data analysed by two-way ANOVA with Tukey's multiple comparisons test on duplicate samples. (0) Quantitation of cJUN expression by densitometry. Band intensity normalised to GAPDH. Data analysed by two-way ANOVA with Tukey's multiple comparisons test on duplicate samples

arrest and estradiol rescue in pLenti cells, but levels are dramatically reduced with MAP2K7 knockout.

Additionally, we assessed the dynamic change in ER α and MKK7 expression after fulvestrant arrest and estradiol stimulation (Supplementary Fig. 5M-R). MCF-7 and T-47D pLenti and $MAP2K7^{-/-}$ cells had a similar fluctuation in ER α expression upon treatment with fulvestrant and estradiol (Supplementary Fig. 5O, Q). MKK7 expression was not altered by fulvestrant or estradiol treatment in pLenti or $MAP2K7^{-/-}$ MCF-7 or T-47D cells (Supplementary Fig. 5P, R).

Finally, we examined the relationship between JNK pathway genes and *JUN/JUND* expression in primary ER+ breast cancers from the TCGA (n = 812) (Supplementary Fig. 5S-V) [37]. MAP2K7 was positively correlated with JUN and JUND expression, whereas MAP2K4, MAPK8 and MAPK9 were negatively correlated with JUN and JUND expression. Therefore, MAP2K7 is a probable primary driver of JUN stability via the JNK pathway in ER+ breast cancer.

Loss of JNK pathway genes and pJNK^{T183/Y185} activity is common in ER+ breast cancer

Our CRISPR screens identified JNK pathway loss, or potential tumour suppressive action, in the context of first-line combination endocrine and CDK4/6 inhibitor treatment for ER+ breast cancer. Since the JNK pathway is associated with both oncogenic and tumour suppressive functions depending on the tumour type [53] we systematically examined patient cohorts to elucidate the relationship of the JNK pathway and its individual genes in ER+ breast cancer.

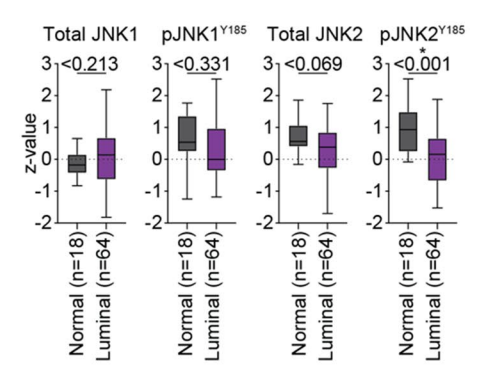
Firstly, we examined the expression and phosphorylation of JNK1 (*MAPK8*) and JNK2 (*MAPK9*) in ER+ breast cancer using UALCAN data [40]. In normal tissue and primary luminal ER+ breast cancers, JNK1 and JNK2 proteins are expressed at similar levels (Fig. 6A). However, we observed that pJNK2^{Y185} but not pJNK1^{Y185} can occur at much lower levels, with pJNK2^{Y185} expressed significantly lower in primary ER+ breast cancers than normal tissues (Fig. 6A). These data indicate that JNK pathway downregulation is common in primary ER+ breast cancer.

Next, we examined copy number alterations in JNK pathway genes, including those identified in our CRISPR/ Cas9 screens, in primary and metastatic ER+ breast cancer genomic datasets [36-38]. JNK pathway genes were generally not altered in primary disease, except for low frequency deletion of MAP2K4 (Fig. 6B). There was a higher rate of loss of JNK pathway genes in metastatic disease with significantly more gene deletions in MAP3K11, MAP2K7, MAPK8, MAPK9 and JUN, as well as significant amplification events, indicating the potential for the pathway to be both oncogenic and tumour suppressive in this context (Fig. 6B). By contrast, ESR1 amplification, which is a known oncogenic event in advanced ER+ breast cancer occurred exclusively in the metastatic setting, whereas ESR1 deletion was notably absent (Fig. 6B).

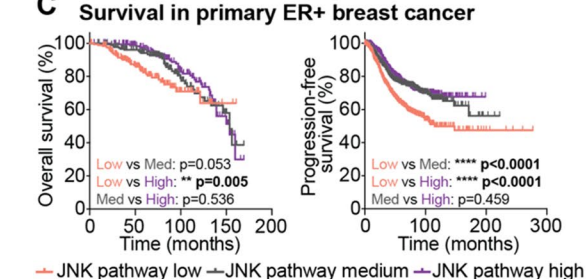
Low expression of pJNK^{T183/Y185} correlates with poor survival in ER+ breast cancer patients treated with endocrine therapy and/or CDK4/6 inhibition

Next, we assessed the association between JNK pathway activation and prognosis in ER+ breast cancer. We

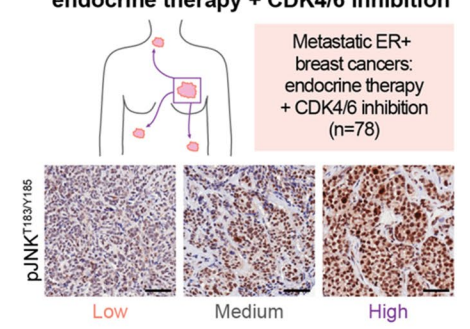
JNK and pJNK^{Y185} expression in normal breast and primary ER+ breast cancer



Survival in primary ER+ breast cancer



pJNK^{T183/Y185} expression in metastatic ER+ breast cancers treated with endocrine therapy + CDK4/6 inhibition



Survival in metastatic ER+ breast cancer patients treated with endocrine therapy + CDK4/6 inhibition

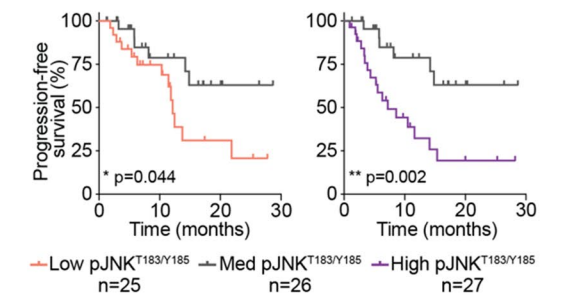
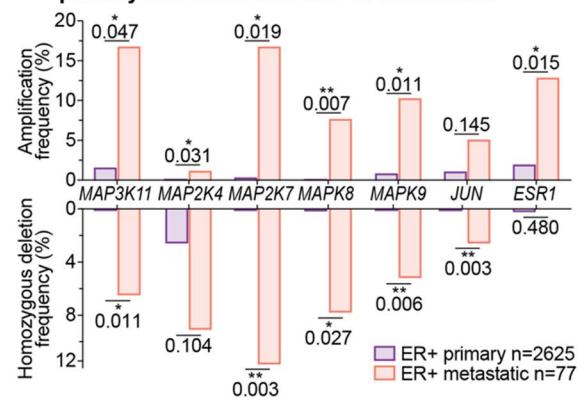
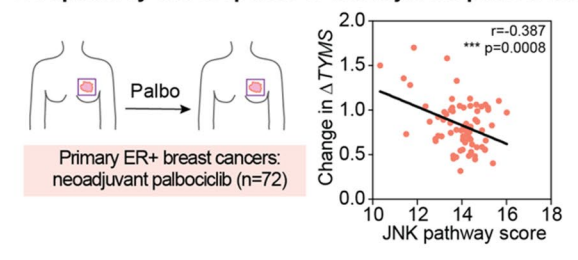


Fig. 6 (See legend on next page.)

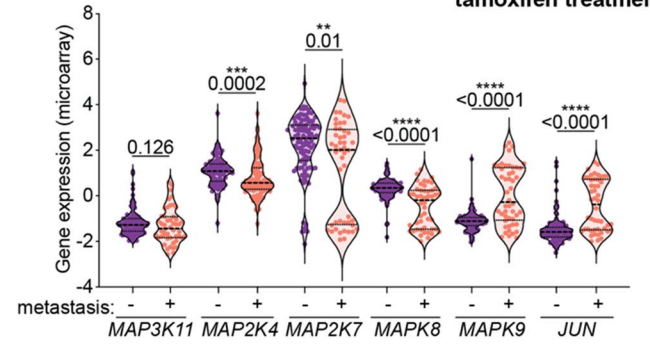
JNK pathway copy number variation in primary and metastatic ER+ breast cancer В



JNK pathway and response to neoadjuvant palbociclib



G Association between JNK genes and metastasis following tamoxifen treatment



Change in tumour proliferation following palbociclib treatment

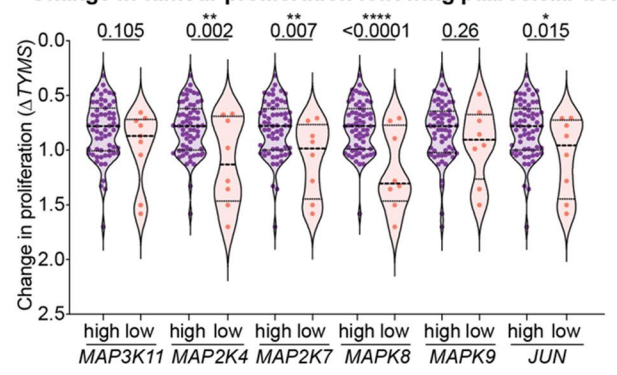


Fig. 6 Depletion of JNK signalling in ER+ breast cancer, and in endocrine therapy/palbociclib resistance (A) JNK1, pJNK1^{Y185} (NP_001265477.1), JNK2, pJNK2^{Y185} (NP_001128516.1) Clinical Proteomic Tumour Analysis Consortium data from the TCGA cohort, showing expression in normal breast tissue (n=18) and luminal breast cancers (n=64). Data analysed by unpaired two-tailed t-test. (B) Copy number status of MAP3K11, MAP2K4, MAP2K7, MAPK8, MAPK9, JUN and ESR1 in primary (TCGA; n = 808 and METABRIC; n = 1817) and metastatic (Metastatic Breast Cancer Project; n = 77) cohorts. Data analysed by unpaired two-tailed t-test. (C) Kaplan-Meier curves of the probability of overall survival and progression-free survival in ER+ breast cancers comparing high, medium, and low tertiles of JNK pathway expression, where JNK pathway is MAP2K7, MAPK8 and MAPK9. Kaplan-Meier analysis performed on pooled breast cancer datasets using KMPlotter [79]. P-value calculated by Log-rank (Mantel-Cox) test. (D) Correlation of JNK pathway with the anti-proliferative response of pre-operative palbociclib (POP) trial ER+ breast cancer patients [43]. Anti-proliferative response determined by change in TYMS mRNA expression between initial biopsy and post-treatment (ΔΤΥΜS) and correlated with JNK signalling (MAP2K7, MAPK8 and MAPK9). Pearson's correlation coefficient shown. (E) Immunohistochemistry analysis of advanced metastatic ER+ breast cancer cohort treated with endocrine therapy + CDK4/6 inhibition. Images of FFPE sections with high, medium, and low pJNK^{T183/Y185} activity. Scale bar = 100 μ m. (F) Kaplan-Meier curves of survival in the endocrine + CDK4/6 inhibitor-treated cohort comparing tertiles of low, medium and high pJNK^{T183/Y185} expression. Significance determined by Log-rank (Mantel-Cox) test. (G) mRNA expression of MAP3K11, MAP2K4, MAP2K7, MAPK8, MAPK9 and JUN stratified into patients who did not develop metastatic disease (no metastasis; n=107) and patients who did (metastasis; n=48). Comparisons between metastatic and non-metastatic by Mann-Whitney unpaired two-tailed t-test. (H) Anti-proliferative response of POP trial ER+ breast cancer patients and association with individual JNK pathway genes. Patients with high (n=64) and low (n=8) JNK pathway gene expression (MAP3K11, MAP2K4, MAPK8, MAPK8, MAPK9 and JUN) were stratified based on TYMS anti-proliferative response. Comparisons between high and low by unpaired two-tailed t-test

used a composite gene expression score of MAP2K7, MAPK8 and MAPK9 since the other genes identified in our CRISPR/Cas9 screens have crosstalk with other signalling pathways. For example, MAP3K11 also regulates ERK signalling [64] and MAP2K4 regulates p38 [52]. Since JNK signalling can be both oncogenic and tumour suppressive, gene expression was split into tertiles. Low JNK signature was associated with worse overall survival compared to high JNK expression (p=0.005), and patients with low JNK-expressing cancers had worse progression-free survival compared to patients with medium expression or high JNK pathway expression (low vs. med: p<0.0001; low vs. high: p<0.0001; Fig. 6C).

Next, we examined the association of JNK signalling with clinical outcomes in patients treated with palbociclib. In the Pre-Operative Palbociclib (POP) trial, patients (n = 72) underwent serial biopsies with intervening neoadjuvant palbociclib treatment [43]. Response to palbociclib was determined as relative changes in proliferation that occurred between the pre-treatment biopsy and post-treatment surgical sample, measured by proliferative marker TYMS. JNK pathway expression (MAP2K7, MAPK8, MAPK9) was negatively correlated with proliferation, indicating that loss of JNK pathway expression was associated with poor response to palbociclib (Fig. 6D).

We examined pJNK^{T183/Y185} activity by IHC in a second cohort of metastatic ER+ breast cancer patients treated with combined endocrine therapy and CDK4/6 inhibition (Supplementary Fig. 6A) [30]. pJNK^{T183/Y185} activity exhibited predominantly nuclear staining which was quantified by H-score. pJNK^{T183/Y185} staining scores were stratified into low, medium and high pJNK^{T183/Y185}-expressing tertiles to examine potential oncogenic and tumour suppressive roles for JNK in these samples (Fig. 6E, Supplementary Fig. 6B). Kaplan-Meier survival analysis showed significantly poorer progression-free survival in patients with low compared

to medium pJNK^{T183/Y185} activity (p = 0.044), and high compared to medium pJNK^{T183/Y185} activity (p = 0.002) (Fig. 6F). There was no significant difference between low and high pJNK^{T183/Y185}-expressing cancers (p = 0.214, graph not shown).

As we had identified that knockout of distinct JNK pathway genes was associated with poor therapeutic response in our CRISPR screens, we next examined the association of individual JNK pathway genes with metastasis-free survival following therapy. We investigated a cohort of breast cancers [41] where 48 of 155 patients (31%) developed distant metastases following 5 years of tamoxifen treatment (Fig. 6G). Patients with low MAP2K4, MAP2K7 or MAPK8 expression or high MAPK9 or JUN in their tumours had greater metastatic frequency following tamoxifen treatment (Fig. 6G). We then examined individual target genes within the POP clinical study, and their association with response. Low expression of MAP2K4, MAP2K7, MAPK8 and JUN was significantly associated with poor response to palbociclib (Fig. 6H).

Discussion

Our study employed an unbiased whole-genome approach to demonstrate that the JNK signalling cascade plays an important role in driving insensitivity to combination endocrine therapy and CDK4/6 inhibition in ER+breast cancer. These findings provide new insights into the multi-faceted roles of JNK signalling and its implications in therapeutic resistance.

The role of JNK activation in ER+ breast cancer is particularly controversial. JNK activation has been shown to drive CDK4/6 inhibitor resistance [65] and is associated with poor prognosis in luminal B type breast cancers [66]. Models of endocrine therapy resistance are reported to have elevated JNK activity, suggesting that JNK signalling is oncogenic in this setting, and that JNK is activated in ER+ breast cancer cells with *ESR1* mutation [67].

Furthermore, JNK knockdown decreases ER+ breast cancer cell proliferation [68], an observation that we also see with MAPK8 or MAPK9 knockdown (Supplementary Fig. 3J). Conversely, mouse models with inactivated JNK signalling have increased tumour incidence [69, 70]. This duality has led to a conflicting rationale to pursue both JNK inhibitors [67] and JNK activators [71] for ER+ breast cancer.

Due to this controversy, we examined both high and low expression of JNK pathway genes across primary and metastatic ER+ breast cancer patient cohorts. We observed that inactivation of JNK signalling, along with low expression of MAP2K7 and MAPK8, were consistently associated with poor outcome or poor drug response in ER+ breast cancer following various treatment regimes. However, high pJNKT183/Y185 activity was also associated with poor outcome in endocrine therapy and CDK4/6 inhibitor-treated patients, and high expression of MAPK9 and JUN associated with increased metastasis in a tamoxifen-treated cohort. These findings underscore the nuanced role of JNK signalling in ER+ breast cancer, where any deviation from normal/medium levels of JNK signalling, be it hyperactivation or suppression was associated with poor outcomes in ER+ breast cancer.

Amplification, deletion and mutation of JNK pathway components, particularly in the metastatic setting, suggest that polyclonal disease may involve simultaneous activation and inactivation of the pathway within individuals. MKK7, a primary kinase in this pathway, emerged as a critical regulator in our CRISPR screens. Interestingly, MAP2K7 has been previously identified as a hit in screens for tamoxifen and fulvestrant resistance [72, 73] though never characterised. Our findings suggest that suppression of JNK signalling, particularly through MAP2K7 loss, is a key element of insensitivity to endocrine therapy and CDK4/6 inhibition. MAP2K7 knockout reduced sensitivity to endocrine therapies and palbociclib in both short- and long-term assays, suggesting that its role extends beyond canonical JNK pathway functions, such as apoptosis induction [74] to include modulation of stress signalling and senescence.

The interplay between JNK and ER signalling may further illuminate the role of JNK signalling in endocrine therapy and CDK4/6 inhibitor insensitivity. Mechanistically, the depletion of JNK signalling appears intrinsically linked to anti-estrogen and estrogen function. JNK1 has been implicated in directly binding promoters in an AP-1/ESR1 complex, moderating ER-directed transcription [68]. Although MAPK8 and MAPK9 knockout did not have profound effects in our models, functional substitution within the pathway and the dominant role of MAP2K7 may explain this observation. Increased expression of AP-1 components, including JUN, have also been observed in models of ER+ breast cancer following CDK4/6 inhibition [75]. JUN, a downstream effector of JNK, has also been implicated as an oncogene in ER+ breast cancer, reinforcing the complexity of JNK's role in modulating ER signalling and therapy insensitivity [76].

Our current understanding of markers of combination resistance is largely based on patient data emerging from clinical trials [43, 46, 47, 50, 77, 78]. However, these studies are constrained by the limited scope of targets analysed, which usually entail gene panels of known or suspected cancer drivers. Notably, the JNK pathway is not represented on these panels apart from MAP2K4. Concerningly, the absence of JNK pathway components in genomic panels could negatively impact patient outcomes when considering therapeutic sequencing before and after CDK4/6 inhibitor use, particularly given the context-dependent effects of the JNK cascade.

Conclusions

We have identified a subset of patients' refractory to combination endocrine therapy and CDK4/6 inhibition exhibit defective JNK pathway signalling. The loss of this pathway disrupts drug-induced stress signalling and impairs therapy-induced senescence induction. We provide the rationale to screen ER+ breast cancers for pJNK^{T183/Y185} and MAP2K7 expression and caution against the use of JNK inhibitors in this setting.

Abbreviations

FDR

AP-1 Activator protein-1 CDK4/6 Cyclin-dependent kinase 4/6 DFGs Differentially expressed genes DMSO Dimethyl sulfoxide FR Estrogen receptor FR+ Estrogen receptor positive **EtOH** Absolute ethanol FBS Fetal bovine serum

False discovery rate **FFPF** Formalin-fixed paraffin-embedded

gDNA genomic DNA

gRNAs quide RNAs

GIMR Garvan Institute of Medical Research **GSEA** Gene set enrichment analysis IC₅₀ Half-maximal inhibitory concentration

IHC **Immunohistochemistry** JNK c-Jun N-terminal kinase MBCP Metastatic Breast Cancer Project MDS Multidimensional scaling

METABRIC Molecular Taxonomy of Breast Cancer International Consortium

MOI Multiplicity of infection PCR Polymerase chain reaction Ы Propidium jodide

POP Pre-Operative Palbociclib (POP) trial **PVDF** Polyvinylidene fluoride SFM Standard error of the mean sgRNAs Single guide RNAs **TCGA** The Cancer Genome Atlas

VCFG Victorian Centre for Functional Genomics

Supplementary Information

The online version contains supplementary material available at https://doi.or g/10.1186/s13046-025-03466-9.

Supplementary Table 1: sqRNA hits from CRISPR/Cas9 screens

Supplementary Table 2: Common sgRNA hits from CRISPR/Cas9 screens

Supplementary Table 3: RNAseq counts per million

Supplementary Table 4: Transcription factors from RNAseq

Supplementary Fig. 1: Quality control from CRISPR/Cas9 screens and MCF-7 dose response curves (A) Total reads, both mapped and unmapped, across 2 biological CRISPR/Cas9 screens. (B) Gini index (a measure of inequality, with 1 being the most unequal) compared to the starting cell population (T_0) and between replicates. Data in (A and B) were analysed using MAGeCK-VISPR [19]. (C) Dose response curve of MCF-7 cells treated for 5 days with tamoxifen. IC_{50} values were determined by log transforming, normalising, and plotting data with a nonlinear fit of least square analysis. Experiment performed in quadruplicate. (D) Dose response curve of MCF-7 cells treated for 5 days with palbociclib. IC_{50} values were determined by log transforming, normalising, and plotting data with a nonlinear fit of least square analysis. Experiment performed in triplicate. (E) Population size of MCF-7 cells treated for up to 90 days with 500 nM palbociclib (palb), 500 nM tamoxifen + 250 nM palbociclib (tam + palb), or vehicle (tetrahydrofuran). Dotted line indicates starting cell number.

Supplementary Fig. 2: Effect of MAP2K7 knockout on MKK4 and JNK expression (A) Quantitation of MKK4 protein expression in MCF-7 pLenti and MAP2K7^{-/-} (MKK7_1 and MKK7_3) cells by densitometry. Band intensity normalised to respective GAPDH. Data analysed by one-way ANOVA with Tukey's multiple comparisons test. (B) Uncropped Western blots for Fig. 2A. Polyvinylidene fluoride (PVDF) membranes were sliced into smaller sections to incubate with primary antibodies to allow accurate comparison of protein expression within a single sample. Full sections of the sliced membranes from each cropped Western blot are shown. (C) Quantitation of MKK4 protein expression in T-47D pLenti and MAP2K7 (MKK7_1 and MKK7_3) cells by densitometry. Band intensity normalised to respective GAPDH. Data analysed by one-way ANOVA with Tukey's multiple comparisons test. (D) Uncropped Western blots for Fig. 2C. PVDF membranes were sliced into smaller sections to incubate with primary antibodies to allow accurate comparison of protein expression within a single sample. Full sections of the sliced membranes from each cropped Western blot are shown. (E) Quantitation of JNK protein expression in MCF-7 pLenti and MAP2K7^{-/-} (MKK7_1 and MKK7_3) cells by densitometry. Band intensity normalised to respective GAPDH. Data analysed by oneway ANOVA with Tukey's multiple comparisons test. (F) Uncropped Western blots for Fig. 2F. PVDF membranes were sliced into smaller sections to incubate with primary antibodies to allow accurate comparison of protein expression within a single sample. Full sections of the sliced membranes from each cropped Western blot are shown. (G) Quantitation of JNK protein expression in T-47D pLenti and MAP2K7^{-/-} (MKK7_1 and MKK7_3) cells by densitometry. Band intensity normalised to respective GAPDH. Data analysed by one-way ANOVA with Tukey's multiple comparisons test. (H) Uncropped Western blots for Fig. 2H. PVDF membranes were sliced into smaller sections to incubate with primary antibodies to allow accurate comparison of protein expression within a single sample. Full sections of the sliced membranes from each cropped western blot are shown. (I) Uncropped Western blots for Fig. 2K. PVDF membranes were sliced into smaller sections to incubate with primary antibodies to allow accurate comparison of protein expression within a single sample. Full sections of the sliced membranes from each cropped Western blot are shown. (J) Quantitation of pJNK^{T183/Y185} activity in MCF-7 pLenti and MAP2K7^{-/-} (MKK7_1 and MKK7_3) cells treated with 300 nM anisomycin for 0, 30, 60, 90 min by densitometry. Band intensity normalised to respective JNK expression. Data analysed by two-way ANOVA with Tukey's multiple comparisons test. (K) Uncropped Western blots for Fig. 2M. PVDF membranes were sliced into smaller sections to incubate with primary antibodies to allow accurate comparison of protein expression within a single sample. Full sections of the sliced membranes from each cropped Western blot are shown. (L) Quantitation of pJNK^{T183/Y185} activity in T-47D pLenti and MAP2K7-/- (MKK7_1 and MKK7_3) cells treated with 300 nM anisomycin for 0, 30, 60, 90 min by densitometry. Band intensity normalised to respective JNK expression. Data analysed by two-way ANOVA with Tukey's multiple comparisons test. (M) Uncropped Western blots for Fig. 2O. PVDF membranes were sliced into smaller sections to incubate with primary antibodies to allow accurate comparison of protein expression within a single sample. Full sections of the sliced membranes from each cropped Western blot are shown.

Supplementary Fig. 3: Effect of MAP2K7 knockout on cell cycle regulation, and MAPK8 and MAPK9 knockout on proliferation (A) Quantitation of MAP2K7 mRNA in MCF-7 pLenti and MAP2K7-/- (MKK7_1 and MKK7 3) cells treated with 500 nM tamoxifen + 250 nM palbociclib (tam+palb), 25 nM fulvestrant + 125 nM palbociclib (fas+palb) or vehicle (Absolute ethanol (EtOH) and tetrahydrofuran (THF)) for 48 h. Expression normalised to RPLPO and data analysed by two-way ANOVA with Tukey's multiple comparisons test. (B) Quantitation of MAP2K7 mRNA in T-47D pLenti and MAP2K7-/- (MKK7 1 and MKK7 3) cells treated with 500 nM tamoxifen + 250 nM palbociclib (tam+palb), 25 nM fulvestrant + 125 nM palbociclib (fas+palb) or vehicle (EtOH and THF) for 48 h. Expression normalised to RPLPO and data analysed by two-way ANOVA with Tukey's multiple comparisons test. (C) Quantitation of ERa protein expression in MCF-7 pLenti and MAP2K7^{-/-} (MKK7 1 and MKK7 3) cells treated with 500 nM tamoxifen + 250 nM palbociclib (tam + palb), 25 nM fulvestrant + 125 nM palbociclib (fas + palb) or vehicle (EtOH and THF) for 48 h by densitometry. Band intensity normalised to respective GAPDH. Data analysed by two-way ANOVA with Tukey's multiple comparisons test. (D) Uncropped Western blots for Fig. 3A. Polyvinylidene fluoride (PVDF) membranes were sliced into smaller sections to incubate with primary antibodies to allow accurate comparison of protein expression within a single sample. Full sections of the sliced membranes from each cropped Western blot are shown. (E) Quantitation of ERa protein expression in T-47D pLenti and MAP2K7^{-/-} (MKK7 1 and MKK7 3) cells treated with 500 nM tamoxifen + 250 nM palbociclib (tam+palb), 25 nM fulvestrant + 125 nM palbociclib (fas+palb) or vehicle (EtOH and THF) for 48 h by densitometry. Band intensity normalised to respective GAPDH. Data analysed by two-way ANOVA with Tukey's multiple comparisons test. (F) Uncropped Western blots for Figure 3D. PVDF membranes were sliced into smaller sections to incubate with primary antibodies to allow accurate comparison of protein expression within a single sample. Full sections of the sliced membranes from each cropped Western blot are shown. (G) Cell cycle distribution determined by propidium iodide (PI) staining and flow cytometry of MCF-7 pLenti and MAP2K7^{-/-} (MKK7 1 and MKK7 3) cells treated with 500 nM tamoxifen + 250 nM palbociclib (tam + palb), 25 nM fulvestrant + 125 nM palbociclib (fas + palb) or vehicle (EtOH and THF) for 48 h. No significant changes in cell cycle distribution between pLenti and MAP2K7^{-/-} cells were observed when analysed with χ^2 test. Experiment performed in triplicate. (H) Cell cycle distribution determined by PI staining and flow cytometry of T-47D pLenti and MAP2K7^{-/-} (MKK7_1 and MKK7_3) cells treated with 500 nM tamoxifen + 250 nM palbociclib (tam + palb), 25 nM fulvestrant + 125 nM palbociclib (fas + palb) or vehicle (EtOH and THF) for 48 h. No significant changes in cell cycle distribution between pLenti and $MAP2K7^{-/-}$ cells were observed when analysed with χ^2 test. Experiment performed in triplicate. (I) Gating strategy for cell cycle analysis by flow cytometry as shown in (G) and (H). (J) MCF-7 pLenti, MAPK8^{-/-} and MAPK9⁻ cells treated with 500 nM tamoxifen + 250 nM palbociclib (tam + palb), 25 nM fulvestrant + 125 nM palbociclib (fas + palb) or vehicle (EtOH and THF) were analysed by time-lapse microscopy using an IncuCyte ZOOM over 7 days. Cell count determined by red fluorescent count, and data analysed by two-way ANOVA with Sidak's multiple comparisons test. Experiment performed in triplicate.

Supplementary Fig. 4: MAP2KT^{-/-} ER+ breast cancer cell lines do not show changes in basal levels of apoptotic proteins, or altered response to BCL-2 inhibition (A) Representative Western blot of MCL-1, PUMA, BIM, BCL-XL, BCL-2 and GAPDH in MCF-7 pLenti and MAP2K7^{-/-} (MKK7_1 and MKK7_3) cells. (B) Quantitation of proteins by densitometry. Band intensity normalised to GAPDH. Data analysed by one-way ANOVA with Tukey's multiple comparisons test. (C) Representative Western blot of MCL-1, PUMA, BIM, BCL-XL, BCL-2 and GAPDH in T-47D pLenti and MAP2K7^{-/-} (MKK7_1 and MKK7_3) cells. (D) Quantitation of proteins by densitometry. Band intensity normalised to GAPDH. Data analysed by one-way ANOVA with Tukey's multiple comparisons test. (E) MCF-7 pLenti and MAP2K7-^{-/-} (MKK7_1 and MKK7_3) cells treated with vehicle or 10

 μM venetoclax for 24 h were stained with FITC-conjugated Annexin V and propidium iodide (PI) and analysed by flow cytometry. Data analysed using FlowJo on duplicate samples. (F) T-47D pLenti and MAP2K7^-/- (MKK7_1 and MKK7_3) cells treated with vehicle or 10 μM venetoclax for 24 h were stained with FITC-conjugated Annexin V and PI and analysed by flow cytometry. Data analysed using FlowJo on duplicate samples. (G) Gating strategy for Annexin V and PI analysis by flow cytometry as shown in (E) and (F), including unstained control and compensation controls for FITC alone and PI alone.

Supplementary Fig. 5: Estradiol induction and JUN/JUND expression with MAP2K7 loss (A) Quantitation of JUN, JUND and ATF3 mRNA in MCF-7 pLenti and $MAP2K7^{-/-}$ (MKK7_1 and MKK7_3) cells treated with 500 nM tamoxifen + 250 nM palbociclib (tam + palb), 25 nM fulvestrant + 125 nM palbociclib (fas + palb) or vehicle (Absolute ethanol (FtOH) and tetrahydrofuran (THF)) for 48 h. Expression normalised to RPLPO and data analysed by two-way ANOVA with Tukey's multiple comparisons test, plenti samples were run in duplicate for JUN mRNA. (B) Quantitation of JUN, JUND and ATF3 mRNA in T-47D pLenti and MAP2K7^{-/-} (MKK7_1 and MKK7_3) cells treated with 500 nM tamoxifen + 250 nM palbociclib (tam + palb), 25 nM fulvestrant + 125 nM palbociclib (fas + palb) or vehicle (EtOH and THF) for 48 h. Expression normalised to RPLPO and data analysed by two-way ANOVA with Tukey's multiple comparisons test. pLenti samples were run in duplicate for JUN mRNA. (C) Quantitation of p-cJUN Ser63 activity in MCF-7 pLenti and MAP2K7^{-/-} (MKK7_1 and MKK7_3) cells treated with 500 nM tamoxifen + 250 nM palbociclib (tam + palb), 25 nM fulvestrant + 125 nM palbociclib (fas + palb) or vehicle (EtOH and THF) for 48 h by densitometry. Band intensity normalised to respective cJUN expression. Data analysed by two-way ANOVA with Tukey's multiple comparisons test. (D) Quantitation of JUND protein expression in MCF-7 pLenti and MAP2K7^{-/-} (MKK7 1 and MKK7_3) cells treated with 500 nM tamoxifen + 250 nM palbociclib (tam + palb), 25 nM fulvestrant + 125 nM palbociclib (fas + palb) or vehicle (EtOH and THF) for 48 h by densitometry. Band intensity normalised to respective GAPDH. Data analysed by two-way ANOVA with Tukey's multiple comparisons test. (E) Uncropped Western blots for Fig. 5A. Polyvinylidene fluoride (PVDF) membranes were sliced into smaller sections to incubate with primary antibodies to allow accurate comparison of protein expression within a single sample. Full sections of the sliced membranes from each cropped Western blot are shown. (F) Quantitation of p-CJUN Ser63 activity in T-47D pLenti and $MAP2K7^{-/-}$ (MKK7_1 and MKK7_3) cells treated with 500 nM tamoxifen + 250 nM palbociclib (tam + palb), 25 nM fulvestrant + 125 nM palbociclib (fas + palb) or vehicle (EtOH and THF) for 48 h by densitometry. Band intensity normalised to respective cJUN expression. Data analysed by two-way ANOVA with Tukey's multiple comparisons test. (G) Quantitation of JUND protein expression in T-47D pLenti and MAP2K7^{-/-} (MKK7_1 and MKK7_3) cells treated with 500 nM tamoxifen + 250 nM palbociclib (tam + palb), 25 nM fulvestrant + 125 nM palbociclib (fas + palb) or vehicle (EtOH and THF) for 48 h by densitometry. Band intensity normalised to respective GAPDH. Data analysed by two-way ANOVA with Tukey's multiple comparisons test. (H) Uncropped Western blots for Fig. 5D. PVDF membranes were sliced into smaller sections to incubate with primary antibodies to allow accurate comparison of protein expression within a single sample. Full sections of the sliced membranes from each cropped Western blot are shown. (I) Cell cycle distribution determined by propidium iodide (PI) staining and flow cytometry of MCF-7 pLenti and MAP2K7^{-/-} (MKK7_1 and MKK7_3) cells treated with 10 nM fulvestrant for 48 h and stimulated with 100 nM 17β-estradiol for 12 h and 24 h. No significant changes in cell cycle distribution between pLenti and $MAP2K7^{-/-}$ cells were observed when analysed with χ^2 test. Experiment performed in duplicate. (J) Cell cycle distribution determined by PI staining and flow cytometry of T-47D pLenti and MAP2K7^{-/-} (MKK7_1 and MKK7 3) cells treated with 10 nM fulvestrant for 48 h and stimulated with 100 nM 17 β -estradiol for 12 h and 24 h. No significant changes in cell cycle distribution between pLenti and MAP2K7^{-/-} cells were observed when analysed with χ^2 test. Experiment performed in singlet. (K) Quantitation of p-cJUNSer63 activity in MCF-7 pLenti and MAP2K7-/- (MKK7_1 and MKK7_3) cells treated with 10 nM fulvestrant (fas) and 100 nM 17βestradiol (E2) by densitometry. Band intensity normalised to respective cJUN expression. Data analysed by two-way ANOVA with Tukey's multiple comparisons test on duplicate samples. (L) Quantitation of p-c/JUNSer63 activity in T-47D pLenti and $MAP2K7^{-/-}$ (MKK7_1 and MKK7_3) cells treated with 10 nM fulvestrant (fas) and 100 nM 17β-estradiol (E2) by densitometry. Band intensity normalised to respective cJUN expression. Data analysed by two-way ANOVA with Tukey's multiple comparisons test on duplicate samples. (M) Uncropped Western blots for Fig. 5H. PVDF membranes were sliced into smaller sections to incubate with primary antibodies to allow accurate comparison of protein expression within a single sample. Full sections of the sliced membranes from each cropped western blot are shown. (N) Uncropped Western blots for Fig. 5L. PVDF membranes were sliced into smaller sections to incubate with primary antibodies to allow accurate comparison of protein expression within a single sample. Full sections of the sliced membranes from each cropped Western blot are shown. (O) Quantitation of ERa protein expression in MCF-7 pLenti and MAP2K7^{-/-} (MKK7_1 and MKK7_3) cells treated with 10 nM fulvestrant (fas) and 100 nM 17β -estradiol (E2). Band intensity normalised to respective GAPDH. Data analysed by two-way ANOVA with Tukey's multiple comparisons test. (P) Quantitation of MKK7 protein expression in MCF-7 pLenti and MAP2K7^{-/-} (MKK7_1 and MKK7_3) cells treated with 10 nM fulvestrant (fas) and 100 nM 17β -estradiol (E2). Band intensity normalised to respective GAPDH. Data analysed by two-way ANOVA with Tukey's multiple comparisons test. (Q) Quantitation of ERa protein expression in T-47D pLenti and $\it MAP2K7^{-/-}$ (MKK7_1 and MKK7_3) cells treated with 10 nM fulvestrant (fas) and 100 nM 17β-estradiol (E2). Band intensity normalised to respective GAPDH. Data analysed by two-way ANOVA with Tukey's multiple comparisons test. (R) Quantitation of MKK7 protein expression in T-47D pLenti and MAP2K7^{-/-} (MKK7_1 and MKK7_3) cells treated with 10 nM fulvestrant (fas) and 100 nM 17β -estradiol (E2). Band intensity normalised to respective GAPDH. Data analysed by two-way ANOVA with Tukey's multiple comparisons test. (S) Expression of JUN and JUND in primary ER+ breast cancers from the TCGA cohort (n = 812) compared to MAP2K7 expression. Pearson's correlation coefficient shown. (T) Expression of JUN and JUND in primary ER+ breast cancers from the TCGA cohort (n=812) compared to MAP2K4 expression. Pearson's correlation coefficient shown. (U) Expression of JUN and JUND in primary ER+ breast cancers from the TCGA cohort (n = 812) compared to MAPK8 expression. Pearson's correlation coefficient shown. (V) Expression of JUN and JUND in primary ER+ breast cancers from the TCGA cohort (n = 812) compared to MAPK9 expression. Pearson's correlation coefficient shown.

Supplementary Fig. 6: patient cohort evaluation (A) Flow diagram showing the number of formalin-fixed paraffin-embedded samples from endocrine therapy + CDK4/6 inhibitor-treated ER + patients that were stained with pJNK^{T183/Y185} antibody for immunohistochemistry (IHC) analysis. (B) The distribution of IHC tumour H-scores for pJNK^{T183/Y185} activity split into high, medium, and low.

Acknowledgements

We extend our gratitude to consumer advocates Vanessa Smith and Anny Friis for their feedback and advice during the project. This study was supported by the following facilities at the Garvan Institute of Medical Research: Australian BioResource, Biological Testing Facility, Garvan Molecular Genetics, Garvan Sequencing Platform, Garvan-Weizmann Centre for Cellular Genomics Flow Facility, Tissue Culture Facility under Gillian Lehrbach and Ruth Lyons, and the Garvan Histology Core Facility under Anaiis Zaratzian. Next-generation sequencing for CRISPR/Cas9 screens were performed at the Molecular Genomics Core facility at Peter MacCallum Cancer Centre. We would like to thank Dr Twishi Gulati and the Victorian Centre for Functional Genomics for their expertise and support with CRISPR/Cas9 screening.

Author contributions

Conceptualisation: S. A, C. E. C; Investigation: S. A, C. S. L, K. J. F, C. E. W, Z. P, A. L. C, C. L. A; Methodology: S. A, C. S. L, K. J. F, D. A. R, D. R. C, I. N, K. J. S, P. T, C. E. G; Software: S. A, J. R; Formal analysis: S. A, C. L. A, E. K. A. M, H. J. D, C. E. C; Bioinformatics analysis: L. E; Resources: K. J. S, H. J. D; Writing — Original Draft: S. A, C. E. C; Writing — Review & Editing: S. A, N. P, H. H. M, E. L, T. E. H, C. E. C; Supervision: S. A, C. E. C; Funding acquisition: C. E. C. All authors reviewed the manuscript.

Funding

This study was supported by a National Breast Cancer Foundation IIRS grant (2022/IIRS070). S.A. was supported by the Australian Government

Research Training Program Scholarship and Estée Lauder Breast Cancer Award. The Victorian Centre for Functional Genomics (K.J.S.) is funded by the Australian Cancer Research Foundation (ACRF), Phenomics Australia, through funding from the Australian Government's National Collaborative Research Infrastructure Strategy (NCRIS) program, the Peter MacCallum Cancer Centre Foundation and the University of Melbourne Collaborative Research Infrastructure Program. C.E.C is the recipient of the Lysia O'Keefe Fellowship, and was supported by the Mavis Robertson Fellowship and a Cancer Institute NSW Fellowship (CDF1071).

Data availability

RNAseq data supporting the findings of this study have been deposited into the NCBI Gene Expression Omnibus (GEO) repository under accession code: GSE289411. The remaining data are available within the Article or Supplementary Information. The patient data presented in Figure 6E/F including survival analyses and immunohistochemistry data will not be publicly available to protect patient privacy, and further inquiries can be made to the corresponding author: C. E. Caldon, email address: l.caldon@garvan.org. au.

Declarations

Ethics approval and consent to participate

All animal work was performed in compliance with the Australian Code of Practice for the Care and Use of Animals for Scientific Purposes (National Health and Medical Research Council). The protocol and study end points were approved by the St. Vincent's Health Precinct and GIMR Animal Ethics Committee (ARA 21/09).

Consent for publication

N/A.

Competing interests

E. L provides advisory board services to AstraZeneca, Gilead, Lilly, MDS, Novartis, Pfizer, Roche, and received royalties from Walter and Eliza Hall Institute.

Author details

¹Garvan Institute of Medical Research, Darlinghurst, Sydney, NSW, Australia

²St Vincent's Clinical School, Faculty of Medicine, UNSW Sydney, Sydney, NSW, Australia

³Victorian Centre for Functional Genomics, Peter MacCallum Cancer Centre, Melbourne, VIC, Australia

⁴Sir Peter MacCallum Department of Oncology, Department of Biochemistry and Pharmacology, University of Melbourne, Melbourne, VIC, Australia

⁵Dame Roma Mitchell Cancer Research Adelaide Medical School Laboratories, University of Adelaide, Adelaide, Australia

⁶Department of Anatomical Pathology, NSW Health Pathology, St George Hospital, Sydney, NSW, Australia

⁷St George & Sutherland Campus, School of Clinical Medicine, UNSW Sydney, Sydney, NSW, Australia

⁸Department of Molecular Medicine, Cancer Research Unit, University of Southern Denmark, Odense, Denmark

⁹Department of Oncology, Odense University Hospital, Odense, Denmark

Received: 15 April 2025 / Accepted: 3 July 2025 Published online: 19 August 2025

References

- Finn RS, et al. Palbociclib and letrozole in advanced breast Cancer. N Engl J Med. 2016;375:1925–36. https://doi.org/10.1056/NEJMoa1607303.
- Hortobagyi GN, et al. Ribociclib as First-Line therapy for HR-Positive, advanced breast Cancer. N Engl J Med. 2016;375:1738–48. https://doi.org/10.1056/NEJ Moa1609709.
- Goetz MP, et al. MONARCH 3: abemaciclib as initial therapy for advanced breast cancer. J Clin Oncology: Official J Am Soc Clin Oncol. 2017;35:3638–46. https://doi.org/10.1200/JCO.2017.75.6155.

- Sledge GW, et al. The effect of abemaciclib plus fulvestrant on overall survival in hormone receptor–positive, ERBB2-negative breast cancer that progressed on endocrine therapy—MONARCH 2: a randomized clinical trial. JAMA Oncol. 2020;6:116–24.
- Slamon D, et al. Ribociclib plus fulvestrant for postmenopausal women with hormone receptor-positive, human epidermal growth factor receptor 2-negative advanced breast cancer in the phase III randomized MONALEESA-3 trial: updated overall survival. Ann Oncol. 2021;32:1015–24.
- Hortobagyi GN, et al. Overall survival with ribociclib plus letrozole in advanced breast cancer. N Engl J Med. 2022;386:942–50.
- Lu Y-S, et al. Updated overall survival of ribociclib plus endocrine therapy versus endocrine therapy alone in pre-and perimenopausal patients with HR+/HER2-advanced breast cancer in MONALEESA-7: a phase III randomized clinical trial. Clin Cancer Res. 2022;28:851–9.
- Turner NC, et al. Overall survival with Palbociclib and fulvestrant in advanced breast cancer. N Engl J Med. 2018;379:1926–36.
- Slamon D, et al. Ribociclib plus endocrine therapy in early breast cancer. N Engl J Med. 2024;390:1080–91.
- Johnston SR, et al. Abemaciclib plus endocrine therapy for hormone receptor-positive, HER2-negative, node-positive, high-risk early breast cancer (monarchE): results from a Preplanned interim analysis of a randomised, open-label, phase 3 trial. Lancet Oncol. 2023;24:77–90.
- Portman N, et al. Overcoming CDK4/6 inhibitor resistance in ER-positive breast cancer. Endocr Relat Cancer. 2019;26:R15–30. https://doi.org/10.1530/ erc-18-0317
- Milioli H, Alexandrou S, Lim E, Caldon CE. Cyclin E1 and Cyclin E2 in ER+ breast cancer: prospects as biomarkers and therapeutic targets. Endocrinerelated Cancer. 2020;27:R93–112.
- 13. Wander SA, et al. The genomic landscape of intrinsic and acquired resistance to cyclin-dependent kinase 4/6 inhibitors in patients with hormone Receptor–Positive metastatic breast cancer. Cancer Discov. 2020;10:1174–93.
- 14. Li Z, et al. Loss of the FAT1 tumor suppressor promotes resistance to CDK4/6 inhibitors via the Hippo pathway. Cancer Cell. 2018;34:893–905. e898.
- Bankhead P, et al. QuPath: open source software for digital pathology image analysis. Sci Rep. 2017;7:1–7.
- Caldon CE, et al. Estrogen regulation of Cyclin E2 requires Cyclin D1 but not c-Myc. Mol Cell Biol. 2009;29:4623–39. https://doi.org/10.1128/MCB.00269-09.
- Livak KJ, Schmittgen TD. Analysis of relative gene expression data using realtime quantitative PCR and the 2–ΔΔCT method. Methods 2001;25:402-408.
- Doench JG, et al. Optimized SgRNA design to maximize activity and minimize off-target effects of CRISPR-Cas9. Nat Biotechnol. 2016;34:184–91. https://doi. org/10.1038/nbt.3437.
- Li W, et al. Quality control, modeling, and visualization of CRISPR screens with MAGeCK-VISPR. Genome Biol. 2015;16:281. https://doi.org/10.1186/s13059-0 15-0843-6.
- Andrews S. FastQC: a quality control tool for high throughput sequence data, 2010).
- 21. Genomics X. Build Notes for Reference Packages, 2020).
- Dobin A, et al. STAR: ultrafast universal RNA-seq aligner. Bioinformatics. 2013;29:15–21.
- Liao Y, Smyth GK, Shi W. FeatureCounts: an efficient general purpose program for assigning sequence reads to genomic features. Bioinformatics. 2014;30:923–30.
- 24. Law CW, Chen Y, Shi W, Smyth G. K. voom: precision weights unlock linear model analysis tools for RNA-seq read counts. Genome Biol. 2014;15:1–17.
- Ritchie ME, et al. Limma powers differential expression analyses for RNAsequencing and microarray studies. Nucleic Acids Res. 2015;43:e47–47.
- Robinson MD, McCarthy DJ, Smyth GK. EdgeR: a bioconductor package for differential expression analysis of digital gene expression data. Bioinformatics. 2010;26:139–40. https://doi.org/10.1093/bioinformatics/btp616.
- 27. Ge SX, Jung D, Yao R. ShinyGO: a graphical gene-set enrichment tool for animals and plants. Bioinformatics. 2020;36:2628–9.
- 28. Lambert SA, et al. The human transcription factors. Cell. 2018;172:650–65.
- Chen T, Zhang H, Liu Y, Liu Y-X, Huang L, EVenn. Easy to create repeatable and editable Venn diagrams and Venn networks online. J Genet genomics = Yi Chuan Xue Bao. 2021;48:863–6.
- Alves CL, et al. Co-targeting CDK4/6 and AKT with endocrine therapy prevents progression in CDK4/6 inhibitor and endocrine therapy-resistant breast cancer. Nat Commun. 2021;12:5112.
- 31. Stenger M, Calculating H-S. The ASCO Post (2015).
- 32. Li J, et al. Explore, visualize, and analyze functional cancer proteomic data using the cancer proteome atlas. Cancer Res. 2017;77:e51–4.

- Li J, et al. TCPA: a resource for cancer functional proteomics data. Nat Methods. 2013;10:1046–7.
- Gao J, et al. Integrative analysis of complex cancer genomics and clinical profiles using the cBioPortal. Sci Signal. 2013;6:pl1. https://doi.org/10.1126/sci signal.2004088.
- Cerami E, et al. The cBio cancer genomics portal: an open platform for exploring multidimensional cancer genomics data. Cancer Discov. 2012;2:401–4. htt ps://doi.org/10.1158/2159-8290.CD-12-0095.
- Curtis C et al. The genomic and transcriptomic architecture of 2,000 breast tumours reveals novel subgroups. Nature 486 (2012).
- Network TCG. A. Comprehensive molecular portraits of human breast tumours. Nature. 2012;490:61–70.
- Jain E et al. The Metastatic Breast Cancer Project: leveraging patient-partnered research to expand the clinical and genomic landscape of metastatic breast cancer and accelerate discoveries. medRxiv, 2023.2006. 2007.23291117 (2023).
- Zhang Y, Chen F, Chandrashekar DS, Varambally S, Creighton CJ. Proteogenomic characterization of 2002 human cancers reveals pan-cancer molecular subtypes and associated pathways. Nat Commun. 2022;13:2669.
- Chandrashekar DS, et al. An update to the integrated cancer data analysis platform. Neoplasia 25. 2022;UALCAN:18–27.
- Chanrion M, et al. A gene expression signature that can predict the recurrence of tamoxifen-treated primary breast cancer. Clin Cancer Res. 2008;14:1744–52. https://doi.org/10.1158/1078-0432.CCR-07-1833.
- Li Q, Birkbak NJ, Gyorffy B, Szallasi Z, Eklund AC. Jetset: selecting the optimal microarray probe set to represent a gene. BMC Bioinformatics. 2011;12:1–7.
- Arnedos M, et al. Modulation of Rb phosphorylation and antiproliferative response to palbociclib: the preoperative-palbociclib (POP) randomized clinical trial. Ann Oncol. 2018;29:1755–62. https://doi.org/10.1093/annonc/mdy20
- Park YH, et al. Longitudinal multi-omics study of Palbociclib resistance in HRpositive/HER2-negative metastatic breast cancer. Genome Med. 2023;15:55.
- Noguchi E, et al. A phase 3 study (PATHWAY) of Palbociclib plus Tamoxifen in patients with HR-positive/HER2-negative advanced breast cancer. NPJ Breast Cancer. 2024;10:76.
- Condorelli R, et al. Polyclonal RB1 mutations and acquired resistance to CDK 4/6 inhibitors in patients with metastatic breast cancer. Annals Oncology: Official J Eur Soc Med Oncol. 2018;29:640–5. https://doi.org/10.1093/annonc/mdx784.
- Costa C, et al. PTEN loss mediates clinical Cross-Resistance to CDK4/6 and PI3Kalpha inhibitors in breast Cancer. Cancer Discov. 2020;10:72–85. https://doi.org/10.1158/2159-8290.CD-18-0830.
- lida M, et al. The p21 levels have the potential to be a monitoring marker for ribociclib in breast cancer. Oncotarget. 2019;10:4907.
- O'Brien NA, et al. Targeting activated PI3K/mTOR signaling overcomes acquired resistance to CDK4/6-based therapies in preclinical models of hormone receptor-positive breast cancer. Breast Cancer Res. 2020;22:89. http s://doi.org/10.1186/s13058-020-01320-8.
- O'Leary B, et al. The genetic landscape and clonal evolution of breast Cancer resistance to Palbociclib plus fulvestrant in the PALOMA-3 trial. Cancer Discov. 2018;8:1390–403. https://doi.org/10.1158/2159-8290.Cd-18-0264.
- 51. Bubici C, Papa S. JNK signalling in cancer: in need of new, smarter therapeutic targets. Br J Pharmacol. 2014;171:24–37.
- 52. Hickson JA, et al. The p38 kinases MKK4 and MKK6 suppress metastatic colonization in human ovarian carcinoma. Cancer Res. 2006;66:2264–70.
- Bode AM, Dong Z. The functional contrariety of JNK. Mol Carcinogenesis: Published Cooperation Univ Tex MD Anderson Cancer Cent. 2007:46:591–8.
- Dhanasekaran DN, Reddy EP. JNK signaling in apoptosis. Oncogene. 2008;27:6245–51. https://doi.org/10.1038/onc.2008.301.
- Cano E, Hazzalin CA, Mahadevan LC. Anisomycin-activated protein kinases p45 and p55 but not mitogen-activated protein kinases ERK-1 and 2 are implicated in the induction of c-fos and c-jun. Mol Cell Biol. 1994;14:7352–62. https://doi.org/10.1128/mcb.14.11.7352.
- Klapp V, et al. Cellular senescence in the response of HR+ breast cancer to radiotherapy and CDK4/6 inhibitors. J Translational Med. 2023;21:110.
- Torres-Guzmán R, et al. Preclinical characterization of abemaciclib in hormone receptor positive breast cancer. Oncotarget. 2017;8:69493.
- Valdez BC, et al. ABT199/venetoclax potentiates the cytotoxicity of alkylating agents and fludarabine in acute myeloid leukemia cells. Oncotarget. 2022:13:319.

- Valdez BC, et al. ABT199/venetoclax synergism with Thiotepa enhances the cytotoxicity of fludarabine, cladribine and Busulfan in AML cells. Oncotarget. 2024;15:220.
- Lenhard WL. Computation of effect sizes. Psychometrica. 2022. https://doi.org/10.13140/RG.2.2.17823.92329.
- Soria-Bretones I, et al. The spindle assembly checkpoint is a therapeutic vulnerability of CDK4/6 inhibitor–resistant ER+ breast cancer with mitotic aberrations. Sci Adv. 2022;8:eabq4293.
- Gori I, et al. Tumor necrosis factor-α activates Estrogen signaling pathways in endometrial epithelial cells via Estrogen receptor α. Mol Cell Endocrinol. 2011;345:27–37.
- Dahlman-Wright K, et al. Interplay between AP-1 and Estrogen receptor α in regulating gene expression and proliferation networks in breast cancer cells. Carcinogenesis. 2012;33:1684–91.
- Chadee DN, Kyriakis JM. MLK3 is required for mitogen activation of B-Raf, ERK and cell proliferation. Nat Cell Biol. 2004;6:770–6.
- Griffiths JI, et al. Serial single-cell genomics reveals convergent subclonal evolution of resistance as patients with early-stage breast cancer progress on endocrine plus CDK4/6 therapy. Nat cancer. 2021;2:658–71.
- Chen L, et al. The prognostic significance of anisomycin-activated phosphoc-Jun NH2-terminal kinase (p-JNK) in predicting breast cancer patients' survival time. Front Cell Dev Biology. 2021;9:656693.
- Taya M et al. Beyond endocrine resistance: Estrogen receptor (ESR1) activating mutations mediate chemotherapy resistance through the JNK/c-Jun MDR1 pathway in breast cancer. (2024).
- Sun M, et al. Estrogen regulates JNK1 genomic localization to control gene expression and cell growth in breast cancer cells. Mol Endocrinol. 2012;26:736–47.
- Girnius N, Edwards YJ, Garlick DS, Davis RJ. The cJUN NH2-terminal kinase (JNK) signaling pathway promotes genome stability and prevents tumor initiation. Elife. 2018;7:e36389.
- Schramek D, et al. The stress kinase MKK7 couples oncogenic stress to p53 stability and tumor suppression. Nat Genet. 2011;43:212–9.
- 71. Ahn S, Kwon A, Oh Y, Rhee S, Song WK. Microtubule acetylation-specific inhibitors induce cell death and mitotic arrest via JNK/AP-1 activation in triple-negative breast cancer cells. Mol Cells. 2023;46:387–98.
- Iorns E, et al. Identification of CDK10 as an important determinant of resistance to endocrine therapy for breast cancer. Cancer Cell. 2008;13:91–104.
- Hany D, Vafeiadou V, Picard D. CRISPR-Cas9 screen reveals a role of purine synthesis for Estrogen receptor α activity and Tamoxifen resistance of breast cancer cells. Sci Adv. 2023;9:eadd3685.
- Franco YL, et al. A quantitative systems Pharmacological approach identified activation of JNK signaling pathway as a promising treatment strategy for refractory HER2 positive breast cancer. J Pharmacokinet Pharmacodyn. 2021;48:273–93.
- Watt AC, et al. CDK4/6 inhibition reprograms the breast cancer enhancer landscape by stimulating AP-1 transcriptional activity. Nat Cancer. 2021;2:34–48
- He H, et al. c-Jun/AP-1 overexpression reprograms ERα signaling related to Tamoxifen response in ERα-positive breast cancer. Oncogene. 2018:37:2586–600.
- Turner NC et al. Cyclin E1 Expression and Palbociclib Efficacy in Previously Treated Hormone Receptor-Positive Metastatic Breast Cancer. *Journal of clinical oncology: official journal of the American Society of Clinical Oncology*, Jco1800925. https://doi.org/10.1200/jco.18.00925 (2019).
- Formisano L, et al. Aberrant FGFR signaling mediates resistance to CDK4/6 inhibitors in ER+ breast cancer. Nat Commun. 2019;10:1373. https://doi.org/1 0.1038/s41467-019-09068-2.
- Gyorffy B, et al. An online survival analysis tool to rapidly assess the effect of 22,277 genes on breast cancer prognosis using microarray data of 1,809 patients. Breast Cancer Res Treat. 2010;123:725–31. https://doi.org/10.1007/s1 0549-009-0674-9.

Publisher's note

Springer Nature remains neutral with regard to jurisdictional claims in published maps and institutional affiliations.